Unified theory of the impurity and phonon scattering effects on Auger recombination in semiconductors

Masumi Takeshima
Semiconductor Laboratory, Matsushita Electronics Corporation, Takatsuki, Osaka, Japan
(Received 27 October 1981)

I have developed a theory of impurity- and phonon-assisted Auger recombination in semiconductors. The theory is based on the Green's function, which is derived by taking into account both the impurity scattering and the phonon scattering. The function is shown as a test to explain well the conductivity data of heavily doped n-type Ge. The theory is applied to p-type materials of GaAs, InP, GaSb, and InAs for acceptor concentrations between 10^{17} and 10^{20} cm^{-3} and for temperatures between 77 and 500 K. Those materials are typical in that the band-gap energy E_G is much larger than the spin splitoff energy Δ_0 for the former two materials and these are comparable for the latter two. It is shown that the impurity- and phonon-assisted Auger recombination is predominant in materials with $E_G >> \Delta_0$ for the acceptor concentrations between 10^{17} and 10^{19} cm^{-3} and/or for the temperatures below 300 K. Except for these cases the Auger recombination is roughly or well described by the pure collision Auger process. On the other hand, at light-doping levels the Auger recombination assisted by the phonon scattering alone is predominant for all materials. It is stressed that an analysis based on the pure collision Auger process leads to erroneous numerical results for most cases of practical interest.

I. INTRODUCTION

The Auger recombination of the minority carriers in semiconductors is an important nonradiative process, which cannot be suppressed by reduction of impurities other than dopants. A number of theoretical and experimental investigations[1] have been made on the basis of the pure collision Auger process since the successful work by Beatie and Landsberg.[2] However, the pure collision Auger process alone is insufficient to explain the recombination rate especially at low temperatures[3–6] and/or in heavily doped materials.[7] In order to give a better explanation the phonon-assisted Auger recombination[5,8–11] and the impurity-assisted Auger recombination[12] (referred to as I) have been proposed. Though these were found to be promising proposals, the theories given there are incomplete for the reasons that follow.

In the earlier theory of the phonon-assisted Auger recombination, the phonon scattering was taken into account in terms of the second-order perturbation treatment with respect to the electron-phonon interaction as well as the electron-electron interaction. Since the energy denominator involved in the theory can be zero, the divergence difficulty arose. The difficulty was avoided by making the approximation that the energy denominator was replaced by the value evaluated at the threshold of the Auger process. Thus, the approximation is valid only under some restrictive conditions. The divergence difficulty was avoided by the present author on the basis of the Green's-function formalism[13] (referred to as II).

On the other hand, the theory of the impurity-assisted Auger recombination was developed using the same formalism by the present author in I. Here, the approximation used in the limit of the low-impurity concentration and weak scattering is not valid for cases of practical interest: The theory provides only the qualitative description of the Auger process. Furthermore, we must take into account both the impurity and the phonon assistance on an equal basis as long as the temperature is moderately high.

The present paper describes a theory of the minority-carrier lifetime of the Auger recombination, which is based on unified treatment of the impurity and phonon scattering effects. As for the impurity scattering effect the Green's function is derived under the restrictive condition that impurity potential is sufficiently slow with respect to spatial dependence. Though this condition is not satisfied for the band-gap region, the theory is useful for the intraband region, whose contribution to the Auger process is predominant.

The theory is applied to p-type GaAs, p-type InP, p-type GaSb, and p-type InAs for acceptor

concentrations between 10^{17} and 10^{20} cm^{-3} and for temperatures between 77 and 500 K. Those materials are typical in that the band-gap energy E_G is much larger than the spin splitoff energy Δ_0 for the former two materials and these are comparable for the latter two. The threshold energy for the pure collision process, which takes a finite value for $E_G >> \Delta_0$, is absolutely or nearly zero for $E_G \lesssim \Delta_0$ so that the rate of the pure collision Auger recombination is known[14] to be especially large for $E_G \lesssim \Delta_0$. On the other hand, the impurity and phonon scattering are efficient not only in reducing the threshold energy but also in broadening the band states. This suggests that the Auger recombination is enhanced by moderately strong scattering in the case of $E_G \lesssim \Delta_0$ as well as in the case of $E_G >> \Delta_0$. In Fig. 1 we show the Auger recombination called the CHHS process, which occurs among the conduction band (CB), the heavy-hole band (HB), and the spin splitoff band (SB).

II. MODEL AND BASIC FORMULATION

The expression for the minority carrier lifetime of the Auger recombination, which is given in terms of the retarded Green's function including phonon scattering effect, was given in I. The expression is also useful to the present case only if we use the average Green's function which includes both impurity and phonon scattering effects. Since especially at high doping levels the theory of the impurity scattering has not yet been very well established, we must find out the practical way to treat this problem. First, we define our model by writing down the Hamiltonian as

$$H = H_e + H_{\text{ph}} + H_{e\text{-ph}} + H_{e\text{-}i} + H_{e\text{-}e} \ . \tag{2.1}$$

Here H_e, H_{ph}, $H_{e\text{-ph}}$, $H_{e\text{-}i}$, and $H_{e\text{-}e}$ are the Hamiltonians for the band electrons, the phonons, the electron-phonon interaction, the electron-impurity interaction, and the electron-electron interaction. We assume $H_e + H_{\text{ph}}$ and $H_{e\text{-}i} + H_{e\text{-ph}} + H_{e\text{-}e}$ to be the unperturbed Hamiltonian and the perturbation, respectively. The explicit forms of the Hamiltonians are

$$H_e = \sum_{l\vec{k}\sigma} \xi_{l\vec{k}} a^\dagger_{l\vec{k}\sigma} a_{l\vec{k}\sigma} \ , \tag{2.2}$$

$$H_{\text{ph}} = \sum_{\nu\vec{q}} \omega_{\nu\vec{q}} b^\dagger_{\nu\vec{q}} b_{\nu\vec{q}} \ , \tag{2.3}$$

$$H_{e\text{-ph}} = \frac{1}{\sqrt{V}} \sum_{\nu\vec{q}l\vec{k}\sigma} g_{\nu\vec{q}} (b^\dagger_{\nu\vec{q}} + b_{\nu\vec{q}}) a^\dagger_{l\vec{k}+\vec{q}\sigma} a_{l\vec{k}\sigma} \ , \tag{2.4}$$

$$H_{e\text{-}i} = \frac{Z}{V} \sum_{l\vec{q}\vec{k}\sigma} v(\vec{q}) h(\vec{q}) a^\dagger_{l\vec{k}+\vec{q}\sigma} a_{l\vec{k}\sigma} \ , \tag{2.5}$$

$$H_{e\text{-}e} = \frac{1}{2V} \sum_{\substack{l_1 l_2 l_3 l_4 \\ \vec{k}\vec{k}'\vec{q}\sigma\sigma'}} v(\vec{q}) \langle l_1 \vec{k}+\vec{q} \,|\, l_4 \vec{k} \rangle \times \langle l_2 \vec{k}' - \vec{q} \,|\, l_3 \vec{k}' \rangle \times a_{l_1 \vec{k}+\vec{q}\sigma} a_{l_2 \vec{k}'-\vec{q}\sigma'} a_{l_3 \vec{k}'\sigma'} a_{l_4 \vec{k}\sigma} \ . \tag{2.6}$$

Here, $a^\dagger_{l\vec{k}\sigma}$, $a^\dagger_{l\vec{k}\sigma}$, and $\xi_{l\vec{k}}$ are the creation operator, the annihilation operator, and the electron energy, respectively, for the electron with the band index l, the wave vector $\vec{k}$, and the spin σ. $b^\dagger_{\nu\vec{q}}$, $b_{\nu\vec{q}}$, and $\omega_{\nu\vec{q}}$ are the creation operator, the annihilation operator, and the phonon energy, respectively, for the phonon with the mode index ν and the wave vector $\vec{q}$. V is the crystal volume. $g_{\nu\vec{q}}/\sqrt{V}$ is the electron-phonon coupling constant, which depends on the band index l though not explicitly shown. $v(\vec{q})/V$ and $Zv(\vec{q})h(\vec{q})/V$ are the Fourier components of the unscreened Coulomb potentials for the electron-electron interaction and the electron-impurity interaction, respectively. Here, we assume that the doped impurities are ionized and of one species with valency $-Z$ with

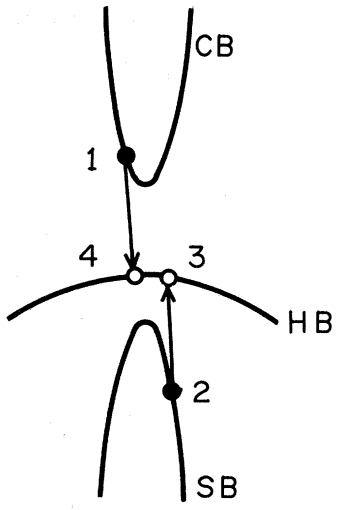

FIG. 1. Auger recombination via the CHHS process among the conduction band, the heavy-hole band, and the spin splitoff band.

respect to the host crystal. $h(\vec{q})$ is the phase factor arising from the interference among scattered waves. We have

$$h(\vec{q})=\sum_{n=1}^{N_i}\exp(-i\vec{q}\cdot\vec{R}_n) \tag{2.7}$$

for N_i impurities which are located at $\vec{R}_n$ $(n=1,2,\ldots,N_I)$. Hereafter we use $i=\sqrt{-1}$. For the electron-electron interaction we take into account the interband scattering but this is neglected for the electron-phonon interaction and for the electron-impurity interaction. $\langle l\vec{k}\,|\,l'\vec{k}'\rangle$ is the overlap integral between the modulating parts of the Bloch functions $|\,l\vec{k}\rangle$ and $|\,l'\vec{k}'\rangle$, which are normalized over the crystal volume. We take $\langle l\vec{k}\,|\,l\vec{k}'\rangle=1$ for the intraband matrix. $v(\vec{q})$ is given by

$$v(\vec{q})=\frac{4\pi e^2}{q^2}\ , \tag{2.8}$$

where e is the electronic charge. As for $g_{\nu\vec{q}}$ we consider the piezoelectric scattering (pe), the acoustic deformation potential scattering (ac), the nonpolar optical deformation potential scattering (npo), and the polar optical phonon scattering (po). The former two and the latter two are for the acoustic phonon mode and for the optical phonon mode, respectively. In Table I we give the expressions[10] of $|\,g_{\nu\vec{q}}\,|^2$ for those scatterings using definitions in Table II. Assuming thermal equilibrium of the system, the electron energy is measured from the Fermi level.

Now we consider the retarded Green's function, which is derived from the Hamiltonian discussed above. In the presence of impurities the function is expressed in terms of two wave vectors $\vec{k}$ and $\vec{k}'$, one energy parameter ω, and position vectors of randomly distributed impurities $\vec{R}_1,\vec{R}_2,\ldots,\vec{R}_{N_i}$ as $G^R(l\vec{k},l\vec{k}';\omega;\vec{R}_1,\vec{R}_2,\ldots,\vec{R}_{N_i})$, whose dependence on the impurity sites comes from $h(\vec{q})$ in Eq. (2.5). Now we take an ensemble average[15–17] over the impurity sites, which is defined as

$$\langle G^R(l\vec{k},l\vec{k}',\omega)\rangle_{\rm av}=\frac{1}{V^{N_i}}\int d\vec{R}_1 d\vec{R}_2\cdots d\vec{R}_{N_i}\,G^R(l\vec{k},l\vec{k}';\omega;\vec{R}_1,\vec{R}_2,\ldots,\vec{R}_{N_i})$$

$$=G^R(l\vec{k},\omega)\Delta(\vec{k}-\vec{k}')\ . \tag{2.9}$$

Here, $\Delta(\vec{q})$ is defined as $\Delta(\vec{q})=1$ if $\vec{q}=0$ and $\Delta(\vec{q})=0$ otherwise. The last step comes from the fact that the space uniformity, which is lost under random distribution of impurities giving $\vec{k}\neq\vec{k}'$, is restored under the average distribution giving momentum conservation $\vec{k}=\vec{k}'$. $G^R(l\vec{k},\omega)$ is the retarded Green's function in the average impurity field, for which the rule of the diagram method is known.[16] The phonon scattering effect can also be incorporated into $G^R(l\vec{k},\omega)$ using the conventional diagram method.[18] It was shown in I that $G^R(l\vec{k},l\vec{k}';\omega;\vec{R}_1,\vec{R}_2,\ldots,\vec{R}_{N_i})$ tends to $\langle G^R(l\vec{k},l\vec{k}',\omega)\rangle_{\rm av}$ as $V\to\infty$. Considering a sufficiently large crystal, all discussions hereafter may be given in terms of $G^R(l\vec{k},\omega)$.

It is rather practical to start from the tempera-

TABLE I. The list of $|\,g_{\nu\vec{q}}\,|^2$.

Scattering mode	$\lvert g_{\nu\vec{q}}\rvert^2$
Piezoelectric scattering (pe)	$\dfrac{e^2P_{\rm pe}^2\omega_{\rm ac}}{2q^2}$
Acoustic deformation potential scattering (ac)	$\dfrac{\Xi^2\omega_{\rm ac}}{2c_l}$
Nonpolar optical deformation potential scattering (npo)	$\dfrac{E_{\rm npo}^2\omega_{\rm op}}{2\bar{c}}$
Polar optical-phonon scattering (po)	$\dfrac{2\pi e^2\omega_{\rm op}}{\epsilon^* q^2}$

TABLE II. Definitions.

$P_{\rm pe}$	dimensionless isotropic piezoelectric constant $P_{\rm pe}^2=\frac{h_{14}^2}{35}\left[\frac{12}{c_l}+\frac{16}{c_t}\right]$
h_{14}	piezoelectric stress tensor
c_l	$=\frac{1}{5}(3c_{11}+2c_{12}+4c_{44})$
c_t	$=\frac{1}{5}(c_{11}-c_{12}+3c_{44})$
$\bar{c}$	$=\frac{1}{3}c_1+\frac{2}{3}c_t$
c_{11},c_{12},c_{44}	elastic stiffness constant
Ξ	effective deformation potential
$E_{\rm npo}$	optical deformation potential
$(\epsilon^*)^{-1}$	$=\epsilon_\infty^{-1}-\epsilon_0^{-1}$
ϵ_∞	high-frequency dielectric constant

ture Green's function (Ref. 18) $\mathcal{G}(l\vec{k},i\omega_m)$, where we define $\omega_m=(2m+1)\pi T$ with m and T as an integer and the thermal energy, respectively. The retarded Green's function is obtained from the relation $G^R(l\vec{k},\omega)=\mathcal{G}(l\vec{k},\omega+i\delta)$, where $\delta\to 0+$. We have a general form

$$\mathcal{G}(l\vec{k},i\omega_m)=\frac{1}{i\omega_m-\xi_{l\vec{k}}-\Sigma(l\vec{k},i\omega_m)} \tag{2.10}$$

as a result of the Dyson's equation,[16,18] which is obtained under the average impurity field. Here $\Sigma(l\vec{k},i\omega_m)$ is the self-energy, which is given by series expansion in terms of the free-particle temperature Green's function

$$\mathcal{G}_0(l\vec{k},i\omega_m)=\frac{1}{i\omega_m-\xi_{l\vec{k}}}\ , \tag{2.11}$$

and of the following three interactions resulting from Eqs. (2.4)–(2.6). The first is the electron-impurity interaction as shown in Fig. 2, where twice followed by twice scattering at two sites are illustrated as an example. The second interaction, shown in Fig. 3, is the electron-electron interaction via the Coulomb potential, for which the overlap integrals are assigned to each vertex. The third interaction, shown in Fig. 4, is the electron-electron interaction via the phonon emission followed by reabsorption. The interaction constant for the last one is $|g_{\nu\vec{q}}|^2\mathcal{D}_0(\nu\vec{q},i\omega_n)$, where

$$\mathcal{D}_0(\nu\vec{q},i\omega_n)=\frac{1}{i\omega_n-\omega_{\nu\vec{q}}}-\frac{1}{i\omega_n+\omega_{\nu\vec{q}}} \tag{2.12}$$

is the free-particle temperature Green's function for the phonon. Here, we define $\omega_n=2n\pi T$ with n as an integer. The free-particle retarded Green's function $D_0^R(\nu\vec{q},\omega)$ for the phonon is obtained from $D_0^R(\nu\vec{q},\omega)=\mathcal{D}_0(\nu\vec{q},\omega+i\delta)$.

Let us take into account the screening by the band electrons on the basis of the electron-hole bubbles shown in Fig. 5. We consider all combinations of the bubbles connected with each other by the broken lines (---) and the wavy lines (~) as shown in Figs. 3 and 4. Then sum of these in-

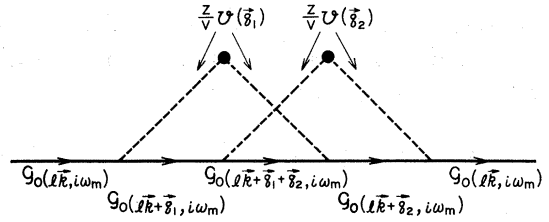

FIG. 2. Fourth-order diagram for the electron-impurity interaction, where the full lines (→), the dashed lines (---), and the points represent the free-particle Green's functions, the interaction constants, and the scattering sites, respectively.

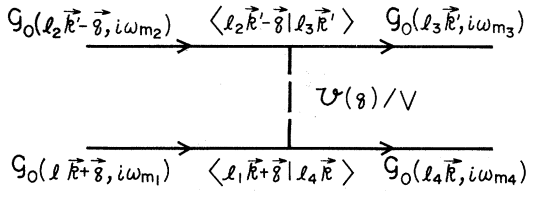

FIG. 3. Diagram for the electron-electron interaction via the Coulomb potential, where the full lines (→) and the broken line (— — —) represent the free-particle Green's functions and the interaction constant, respectively.

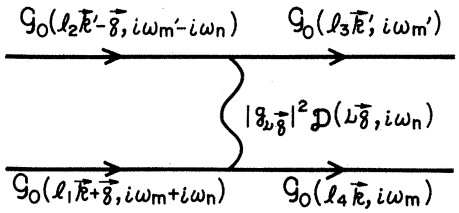

FIG. 4. Diagram for the electron-electron interaction via the phonon emission followed by reabsorption, where the full lines (→) and the wavy lines (〜) represent the free-particle Green's functions and the interaction constant, respectively.

teraction constants (--- and 〜) should be replaced, as shown in II, by the effective interaction constant

$$U_e(\vec{q},i\omega_n)=U_{e\text{-}e}(\vec{q})+U_{e\text{-ph}}(\vec{q},i\omega_n)\ , \tag{2.13}$$

where

$$U_{e\text{-}e}(\vec{q})=\frac{1}{\epsilon(\vec{q})}v(\vec{q}) \tag{2.14}$$

and

$$U_{e\text{-ph}}(\vec{q},i\omega_n)=\left[\frac{\epsilon_0}{\epsilon(\vec{q})}\right]^2|g_{\nu\vec{q}}|^2\mathcal{D}_0(\nu\vec{q},i\omega_n)\ . \tag{2.15}$$

Here we have

$$\epsilon_0=1-v(\vec{q})\sum_{l\neq l'}\chi_{ll'}(0,0) \tag{2.16}$$

and

$$\epsilon(\vec{q})=\epsilon_0-v(\vec{q})\sum_l\chi_{ll}(\vec{q},0)\ , \tag{2.17}$$

where

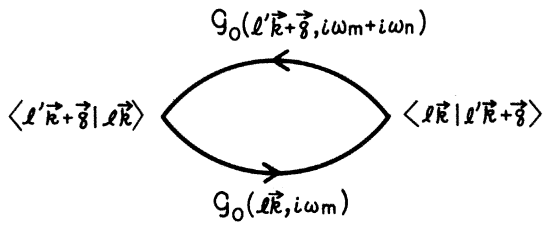

FIG. 5. Electron-hole bubble, where the full lines (→) represent the free-particle Green's functions.

$$\chi_{ll'}(\vec{q},i\omega_n)=2T\sum_{\omega_m}\int\frac{d\vec{k}}{(2\pi)^3}\mathcal{G}(l\vec{k},i\omega_m)\times\mathcal{G}(l'\vec{k}+\vec{q},i\omega_m+i\omega_n)\times|\langle l\vec{k}|l'\vec{k}+\vec{q}\rangle|^2\ . \tag{2.18}$$

$\chi_{ll'}(\vec{q},i\omega_n)$ is obtained from the electron-hole bubbles in Fig. 5 by replacing the free-particle Green's function $\mathcal{G}_0(l\vec{k},i\omega_n)$ by the complete one $\mathcal{G}(l\vec{k},i\omega_n)$. By a similar discussion the interaction constant in Fig. 2 is replaced by the effective interaction constant:

$$U_i(\vec{q},i\omega)=\frac{1}{\epsilon(\vec{q})}Zv(\vec{q})\ . \tag{2.19}$$

Thus, ϵ_0 and $\epsilon(\vec{q})$ represent the dielectric constant of the host crystal and that due to all band electrons, respectively. To calculate $\chi_{ll}(\vec{q},0)$ we use $\mathcal{G}_0(l\vec{k},i\omega_n)$ for the moment in place of $\mathcal{G}(l\vec{k},i\omega_n)$. Then it is shown[18] that

$$\chi_{ll}(\vec{q},0)=2\sum_l\int\frac{d\vec{k}}{(2\pi)^3}\frac{\Theta(\xi_{l\vec{k}+\vec{q}})-\Theta(\xi_{l\vec{k}})}{\xi_{l\vec{k}+\vec{q}}-\xi_{l\vec{k}}}\ , \tag{2.20}$$

where $\Theta(\omega)$ is the Fermi-Dirac distribution function

$$\Theta(\omega)=\frac{1}{\exp\left[\dfrac{\omega}{T}\right]+1}\ . \tag{2.21}$$

We have given the overlap integral as unity for this intraband problem. As for ϵ_0 we use the empirical data. To take $\vec{q}\to 0$ for $\chi_{ll}(\vec{q},0)$ of Eq. (2.17) is known as the Thomas-Fermi approximation, which gives

$$\chi_{ll}(0,0)=2\int\frac{d\vec{k}}{(2\pi)^3}\frac{\partial}{\partial\xi_{l\vec{k}}}\Theta(\xi_{l\vec{k}})\ . \tag{2.22}$$

It is shown later that this is a good approximation in the range of high-carrier concentration. Defining inverse screening length λ as

$$\lambda^2=-\frac{4\pi e^2}{\epsilon_0}\sum_l\chi_{ll}(0,0)\ , \tag{2.23}$$

we obtain

$$\epsilon(\vec{q})=\epsilon_0\left[1+\frac{\lambda^2}{q^2}\right]\ . \tag{2.24}$$

Having constructed the effective interaction con-

stants as in Eqs. (2.13)–(2.19), we are at the position to find the self-energy $\Sigma(l\vec{k},i\omega_m)$ in power series of those constants using the conventional diagram method. At first we consider diagrams made up of the free-particle Green's functions. We classify the diagrams into two groups. One is the sum of terms arising from $U_i(\vec{q})$ and the other is that from $U_e(\vec{q},i\omega_n)$ only. Then replacing the free-particle Green's functions by the complete Green's functions to obtain a better approximation, we write $\Sigma_0+\Sigma_1$ and $\Sigma_2+\Sigma_3$ for the former and for the latter, respectively. For $\Sigma_0+\Sigma_1$ we take all possible diagrams, some of which are illustrated in Fig. 6. For $\Sigma_2+\Sigma_3$ we take all the diagrams which come from the terms of first order in U_e, as shown in Fig. 7, since U_e is small. The self-energy is approximated as

$$\Sigma(l\vec{k},i\omega_m)=\Sigma_0+\Sigma_1(l\vec{k},i\omega_m)+\Sigma_2+\Sigma_3(l\vec{k},i\omega_m) . \tag{2.25}$$

Σ_0 and Σ_2 are shown later to be real constants. Since $\Sigma_0+\Sigma_1$ comes from all irreducible diagrams in series of U_i, it is not necessary any more to incorporate $\Sigma_0+\Sigma_1$ into the Green's functions involved in the diagrams. The Green's function to be used there is

$$\mathcal{G}_1(l\vec{k},i\omega_m)=\frac{1}{i\omega_m-\xi_{l\vec{k}}-\Sigma_2-\Sigma_3(l\vec{k},i\omega_m)} , \tag{2.26}$$

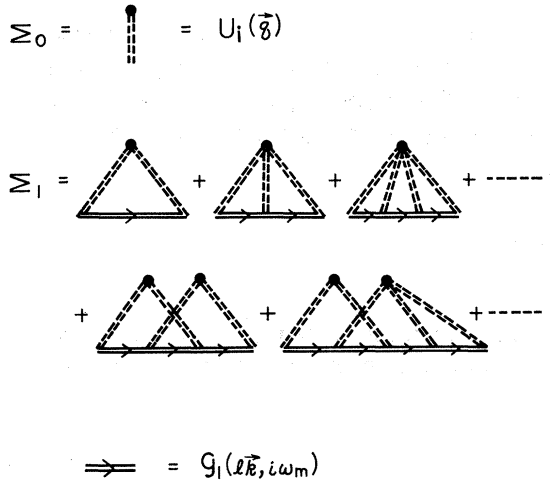

FIG. 6. Self-energy diagrams for Σ_0 and Σ_1, where the double full lines (⇒), the double dashed lines (=⇒), and the points represent the Green's functions $\mathcal{G}_1$, the effective interaction constants, and the scattering sites, respectively.

which involves no impurity scattering effects explicitly.

Let us define

$$\Sigma^R(l\vec{k},\omega)=\Sigma(l\vec{k},\omega+i\delta)$$

and

$$\Sigma_n^R(l\vec{k},\omega)=\Sigma_n(l\vec{k},\omega+i\delta)$$

($n=1,3$). The retarded Green's function is given as

$$G^R(l\vec{k},\omega)=\frac{1}{\omega-\xi_{l\vec{k}}-\Sigma^R(l\vec{k},\omega)} . \tag{2.27}$$

Using the transformation

$$\sum_{\vec{q}}\cdots\rightarrow[V/(2\pi)^3]\int d\vec{q}\cdots ,$$

which is often used hereafter, we obtain from Fig. 7

$$\Sigma_2=-\frac{2}{\pi}\int\frac{d\vec{k}}{(2\pi)^3}U_e(0,0)\int d\omega\,\mathrm{Im}G^R(l\vec{k},\omega)\Theta(\omega)$$
$$=-\frac{2}{\pi}U_{e\text{-}e}(0)\int d\omega\int\frac{d\vec{k}}{(2\pi)^3}\mathrm{Im}G^R(l\vec{k},\omega)\Theta(\omega) . \tag{2.28}$$

The last step is obtained using $U_{e\text{-ph}}(0)=0$, which is found from Eqs. (2.15), (2.24), and Table I. The energy density of states $\rho(\omega)$ is given[17] by

$$\rho(\omega)=-\frac{2}{\pi}\sum_l\int\frac{d\vec{k}}{(2\pi)^3}\mathrm{Im}G^R(l\vec{k},\omega) . \tag{2.29}$$

With n_i as the impurity concentration, the majority carrier concentration $|Z|n_i$ is given by

$$|Z|n_i=\int d\omega\rho(\omega)\Theta'(\omega) . \tag{2.30}$$

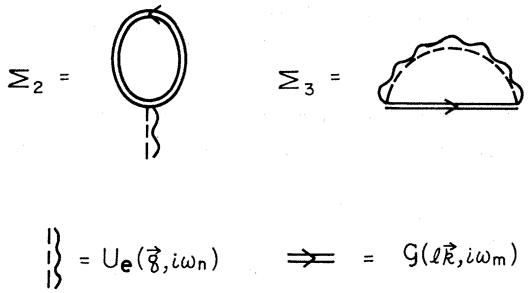

FIG. 7. Self-energy diagrams for Σ_2 and Σ_3, where the double full lines (⇒) and the wavy plus broken lines (≈≈) represent the complete Green's functions $\mathcal{G}$ and the effective interaction constants, respectively.

Here, we have $\Theta'(\omega)=\Theta(\omega)$ when the majority carriers are electrons ($Z<0$) and we have $\Theta'(\omega)=1-\Theta(\omega)$ when they are holes ($Z>0$). From Eqs. (2.8), (2.14), (2.24), and (2.28)–(2.30) we obtain a real constant

$$\Sigma_2=-\frac{4\pi Ze^2n_i}{\epsilon_0\lambda^2}\ . \tag{2.31}$$

When the majority carriers are holes, we omit an additive constant, which is of no interest here. Now we find from Fig. 7

$$\Sigma_3^R(l\vec{k},\omega)=E_x(l\vec{k})+\Sigma_{e\text{-ph}}^R(l\vec{k},\omega)\ , \tag{2.32}$$

where

$$E_x(l\vec{k})=\frac{1}{\pi}\int\frac{d\vec{q}}{(2\pi)^3}\int d\omega\, U_{e\text{-}e}(\vec{k}-\vec{q})\times \mathrm{Im}G^R(l\vec{q},\omega')\Theta(\omega') \tag{2.33}$$

and

$$\Sigma_{e\text{-ph}}^R(l\vec{k},\omega)=\sum_\nu\int\frac{d\vec{q}}{(2\pi)^3}\left[\frac{\epsilon_0}{\epsilon(\vec{k}-\vec{q})}\right]^2\left|g_{\nu\vec{k}-\vec{q}}\right|^2 \times\left[\frac{1}{\pi}\int d\omega' D_0^R(\nu\vec{k}-\vec{q},\omega-\omega')\mathrm{Im}G^R(l\vec{q},\omega')\Theta(\omega') +[1+P(\omega_{\nu\vec{q}})]G^R(l\vec{q},\omega-\omega_{\nu\vec{q}})+P(\omega_{\nu\vec{q}})G^R(l\vec{q},\omega+\omega_{\nu\vec{q}})\right]\ . \tag{2.34}$$

Here $P(\omega)$ is the Bose-Einstein distribution function

$$P(\omega)=\frac{1}{\exp\left[\dfrac{\omega}{T}\right]-1}\ . \tag{2.35}$$

$E_x(l\vec{k})$ is known as the exchange energy and is not very important in this paper. We evaluate this term using the free-particle retarded Green's function $G_0^R(l\vec{k},\omega)=\mathcal{G}_0(l\vec{k},\omega+i\delta)$. We have

$$E_x(l\vec{k})=-\int\frac{d\vec{q}}{(2\pi)^3}U_{e\text{-}e}(\vec{k}-\vec{q})\Theta(\xi_{l\vec{q}})\ . \tag{2.36}$$

If the majority carriers are holes, $\Theta(\xi_{l\vec{q}})$ should be replaced by $\Theta(\xi_{l\vec{q}})-1$. A residual term, which is a constant of no interest here, is omitted. As for $\Sigma_{e\text{-ph}}^R(l\vec{k},\omega)$ we replace $\omega\pm\omega_{\nu\vec{q}}$ by ω as an approximation. Then the first term in the second set of large parentheses in Eq. (2.34) vanishes. $\Sigma_{e\text{-ph}}^R(l\vec{k},\omega)$ represents the phonon emission followed by reabsorption. This can be evaluated using the free-particle retarded Green's function for the reason described in Appendix A. We obtain

$$\Sigma_{e\text{-ph}}^R(l\vec{k},\omega)=\sum_\nu\int\frac{d\vec{q}}{(2\pi)^3}\left[\frac{\epsilon_0}{\epsilon(\vec{q})}\right]^2\left|g_{\nu\vec{q}}\right|^2\frac{1+2P(\omega_{\nu\vec{q}})}{\omega-\xi_{l\vec{k}-\vec{q}}+i\delta}\ . \tag{2.37}$$

Let us now find the expression for $\Sigma_0+\Sigma_1^R(l\vec{k},\omega)$. We consider an irreducible self-energy diagram for n-site scattering. This is expressed after converting from the temperature to the retarded Green's-function formalism as

$$S(m_1,m_2,\ldots,m_n)=\sum_{j=1}^n H_{m_j}\ , \tag{2.38}$$

where m_j is the number of the vertices connected to the jth site under $m_j\geq 1$ and

$$H_m=\sum_{\vec{q}_1,\vec{q}_2,\ldots,\vec{q}_m}\Delta(\vec{Q}_m)\prod_{j=1}^m[U_i(\vec{q}_j)G_1^R(l\vec{k}+\vec{Q}_j,\omega)]/G_1^R(l\vec{k},\omega)\ . \tag{2.39}$$

Here we define $\vec{Q}_m=\sum_{j=1}^{m}\vec{q}_j$ and $G_1^R(l\vec{k},\omega)=\mathcal{G}_1(l\vec{k},\omega+i\delta)$, which is

$$G_1^R(l\vec{k},\omega)=\frac{1}{\omega-\xi_{l\vec{k}}-\Sigma_2-\Sigma_3^R(l\vec{k},\omega)} . \tag{2.40}$$

As discussed in Appendix B, $G_1^R(l\vec{k}+\vec{Q}_j,\omega)$ in Eq. (2.39) can be replaced by $G_1^R(l\vec{k},\omega)$ as an approximation applicable at high-doping levels. Then Eq. (2.38) is rewritten as

$$S(m_1,m_2,\ldots,m_n)=n_i^n[G_1^R(l\vec{k},\omega)]^{M_n-1}\int \mathcal{D}\vec{r}_n\prod_{j=1}^{n}[U_i(\vec{r}_j)]^{m_j} , \tag{2.41}$$

where $\mathcal{D}\vec{r}_n=d\vec{r}_1 d\vec{r}_2\cdots d\vec{r}_n$, $M_n=\sum_{j=1}^{n}m_j$, and $n_i=N_i/V$. In deriving the equation we have used the relation

$$\sum_{\vec{q}_1,\vec{q}_2,\ldots,\vec{q}_m}\Delta(\vec{Q}_m)\prod_{j=1}^{m}U_i(\vec{q}_j)=\frac{1}{V}\int d\vec{r}[U_i(\vec{r})]^m , \tag{2.42}$$

where

$$U_i(\vec{r})=\frac{1}{V}\sum_{\vec{q}}U_i(\vec{q})\exp(i\vec{q}\cdot\vec{r})=\frac{Ze^2}{\epsilon_0 r}\exp(-\lambda r) . \tag{2.43}$$

The last step is obtained from Eqs. (2.19) and (2.24). From the definition in Fig. 6 we have

$$\Sigma_0=S(1)=\frac{4\pi Ze^2 n_i}{\epsilon_0\lambda^2} . \tag{2.44}$$

From Eqs. (2.31) and (2.44) we obtain

$$\Sigma_2+\Sigma_0=0 , \tag{2.45}$$

which represents the charge neutrality condition. Therefore we have

$$\Sigma^R(l\vec{k},\omega)=\Sigma_1^R(l\vec{k},\omega)+\Sigma_3^R(l\vec{k},\omega) . \tag{2.46}$$

To obtain $\Sigma_1^R(l\vec{k},\omega)$ we define $Q_n(m_1,m_2,\ldots,m_n)$ as the number of all irreducible diagrams for n-site scatterings with m_j vertices connected to the jth site. For these n-site scatterings we also define $P_n(m_1,m_2,\ldots,m_n)$ as the number of all diagrams both irreducible and reducible. We have

$$P_n(m_1,m_2,\ldots,m_n)=\frac{1}{n!}\frac{M_n}{\prod_{j=1}^{n}(m_j!)} . \tag{2.47}$$

Noting that $S(m_1,m_2,\ldots,m_n)$ is independent of the positions of G_1^R's appearing in the diagram, the sum of all irreducible diagrams $\bar{Q}$ is written as

$$\bar{Q}=\sum_{n=1}^{\infty}\sum_{m_1,m_2,\ldots,m_n}Q_n(m_1,m_2,\ldots,m_n)\times S(m_1,m_2,\ldots,m_n) . \tag{2.48}$$

The sum of all diagrams both irreducible and reducible $\bar{P}$ is written as

$$\bar{P}=\sum_{n=1}^{\infty}\sum_{m_1,m_2,\ldots,m_n}P_n(m_1,m_2,\ldots,m_n)\times S(m_1,m_2,\ldots,m_n) . \tag{2.49}$$

It is easy to see that

$$\bar{P}=\bar{Q}+G_1^R\bar{Q}\bar{P} . \tag{2.50}$$

Then $\Sigma_0+\Sigma_1^R(=\bar{Q})$ is rewritten as

$$\Sigma_0+\Sigma_1^R=\frac{\bar{P}}{1+G_1^R\bar{P}} . \tag{2.51}$$

We must now calculate $\bar{P}$. Using Eq. (2.41) and abbreviated notation $u_j=G_1^R(l\vec{k},\omega)U_i(\vec{r}_j)$, we obtain

$$\bar{P}=\frac{1}{G_1^R(l\vec{k},\omega)}\sum_{n=1}^{\infty}n_i^n\bar{P}_n , \tag{2.52}$$

with

$$\bar{P}_n=\sum_{m_1,m_2,\ldots,m_n}{}'P_n(m_1,m_2,\ldots,m_n)\times\int\mathcal{D}\vec{r}_n\prod_{j=1}^{n}(u_j^{m_j}) , \tag{2.53}$$

where $\sum'$ means the summation in the range $m_j\geq 1$ $(j=1,2,\ldots,n)$. $\bar{P}_n$ is rewritten as

$$\bar{P}_n=\sum_{M_n=1}^{\infty}\int\mathcal{D}\vec{r}_n\sum_{j=0}^{n-1}(-1)^j\binom{n}{j}\sum{}^{j}P_n(0,\ldots,0,m_{j+1},m_{j+2},\ldots,m_n)u_{j+1}^{m_{j+1}}u_{j+2}^{m_{j+2}}\cdots u_n^{m_n} , \tag{2.54}$$

where $\sum^{j}$ means the summation over $m_{j+1},m_{j+2},\ldots,m_n$ under the restriction $m_{j+1}+m_{j+2}+\cdots+m_n=M_n$. Use of Eq. (2.47) gives

$$\bar{P}_n=\frac{1}{n!}\sum_{M_n=1}^{\infty}\int \mathscr{D}\vec{r}_n \sum_{j=0}^{n-1}(-1)^j\begin{bmatrix}n\\j\end{bmatrix}(u_{j+1}+u_{j+2}+\cdots+u_n)^{M_n}$$

$$=\frac{1}{n!}\int \mathscr{D}\vec{r}_n \sum_{j=0}^{\infty}(-1)^j\begin{bmatrix}n\\j\end{bmatrix}\left[\frac{1}{1-\sum_{p=j+1}^{n}u_p}-1\right]. \tag{2.55}$$

Noting $u_j=G_1^R(l\vec{k},\omega)U_i(\vec{r}_j)$ and Im $[G_1^R(l\vec{k},\omega)]^1>0$, we have

$$\frac{1}{1-\sum_{p=j+1}^{n}u_p}=\frac{1}{iG_1^R(l\vec{k},\omega)}\int_0^{\infty}ds\exp\left[i\left[\frac{1}{G_1^R(l\vec{k},\omega)}-\sum_{p=j+1}^{n}U_i(\vec{r}_p)\right]s\right]. \tag{2.56}$$

Defining

$$h(s)=n_i\int d\vec{r}\{\exp[-isU_i(\vec{r})]-1\}, \tag{2.57}$$

we obtain from Eqs. (2.52), (2.55), and (2.56)

$$\bar{P}=\frac{1}{i[G_1^R(l\vec{k},\omega)]^2}\int_0^{\infty}ds\exp\left[\frac{is}{G_1^R(l\vec{k},\omega)}\right]$$

$$\times\sum_{n=1}^{\infty}\frac{1}{n!}\left[\sum_{j=0}^{n}(-1)^j\begin{bmatrix}n\\j\end{bmatrix}(n_iV)^j[h(s)+n_iV]^{n-j}+(-1)^n(n_iV)^n\right]$$

$$=\frac{1}{i[G_1^R(l\vec{k},\omega]^2}\int_0^{\infty}ds\exp\left[\frac{is}{G_1^R(l\vec{k},\omega)}\right]\sum_{n=1}^{\infty}\frac{1}{n!}[h(s)]^n$$

$$=\frac{1}{i[G_1^R(l\vec{k},\omega)]^2}\int_0^{\infty}ds\exp\left[\frac{is}{G_1^R(l\vec{k},\omega)}\right]\{\exp[h(s)]-1\}. \tag{2.58}$$

Using Eqs. (2.27), (2.45), (2.46), (2.51), and (2.58) we finally obtain

$$G^R(l\vec{k},\omega)=\frac{1}{i}\int_0^{\infty}ds\exp\{is[\omega-\xi_{l\vec{k}}+\Sigma_0-\Sigma_3^R(l\vec{k},\omega)+h(s)]\}. \tag{2.59}$$

It is convenient to rewrite Eq. (2.59) using Eq. (2.44) and defining

$$\Omega=\frac{\epsilon_0}{|Z|e^2\lambda}[\omega-\xi_{l\vec{k}}-\Sigma_3^R(l\vec{k},\omega)], \tag{2.60}$$

$$\gamma=\frac{4\pi n_i}{\lambda^3}, \tag{2.61}$$

and

$$g(\xi)=\int_0^{\infty}dx\,x^2\left[\exp\left[-i\xi\frac{\mathrm{sgn}(Z)}{x}\exp(-x)\right]+i\xi\frac{\mathrm{sgn}(Z)}{x}\exp(-x)-1\right], \tag{2.62}$$

where sgn $(Z)=Z/|Z|$. We have

$$G^R(l\vec{k},\omega)=\frac{\epsilon_0}{|Z|e^2\lambda}\bar{G}^R(\Omega,\gamma;Z), \tag{2.63}$$

where

$$\bar{G}^R(\Omega)=\frac{1}{i}\int_0^{\infty}d\xi\exp[i\xi\Omega+\gamma g(\xi)]. \tag{2.64}$$

In the limit of $\xi \to 0$ we find $g(\xi) = -\frac{1}{4}\xi^2 + O(\xi^3)$. From Eqs. (2.62) and (2.64) we notice the important relation

$$\bar{G}^R(-\Omega^*,\gamma;-Z) = -\bar{G}^R(\Omega,\gamma;Z)^* \ . \tag{2.65}$$

Equation (2.59) is a general expression which involves the electron-impurity scattering effect, the electron-phonon scattering effect, and the electron-electron scattering effect. Especially if we neglect the phonon scattering effect and the exchange energy, i.e., $\Sigma_3^R = -i\delta$, Eq. (2.59) agrees with the expression which was derived[17,19] for the impurity scattering problem by Bonch-Bruevich using a different method. One merit of the method in this paper is that the electron-phonon scattering effect is naturally incorporated into the theory. Another merit is to notice that especially for $\mathrm{Im}\Sigma_3^R(l\vec{k},\omega) = -i\delta$, $\mathrm{Im}G^R(l\vec{k},\omega)$ should be nonzero only in the range

$$[\mathrm{Re}\Omega + \mathrm{sgn}(Z)\gamma]\mathrm{sgn}(Z) > 0 \ . \tag{2.66}$$

This is seen from the discussions in between Eqs. (2.38) and (2.58) noting that

$$\mathrm{Im}\int \mathscr{D}\vec{r}_n \frac{1}{1-\sum_{p=j+1}^{n} u_p} = \mathrm{Re}[G_1^R(l\vec{k},\omega)]^{-1} \int \mathscr{D}\vec{r}_n \delta\left[\mathrm{Re}[G_1^R(l\vec{k},\omega)]^{-1} - Z\sum_{p=j+1}^{n}\left[\frac{e^2}{\epsilon_0 r_p}\exp(-\lambda r_p)\right]\right]$$

does not vanish unless the condition (2.66) is satisfied. The condition (2.66) is important to notice since numerical calculation never gives $\mathrm{Im}G^R(l\vec{k},\omega) = 0$ but often positive values as errors in the range given by the relation (2.66).

III. DISCUSSIONS OF THE IMPURITY SCATTERING

Before going into the discussion of the Auger process, it is necessary to test the validity of the theory of the impurity scattering since this has not been well established as yet. We start from calculating $\mathrm{Im}\bar{G}^R(\Omega,\gamma;Z)$, in terms of which various formulas for physical phenomena are given. The phonon scattering effect is neglected here by taking $\Sigma_3^R = E_x(l\vec{k})$. Then Ω is real. Figure 8 shows the numerical results of $\mathrm{Im}\bar{G}^R(\Omega,\gamma;-1)$, which are calculated from Eq. (2.64). We should have $\mathrm{Im}\bar{G}^R = 0$ for $\Omega > \gamma$ as indicated in the last section and $\mathrm{Im}\bar{G}^R < 0$ for $\Omega < \gamma$ as the retarded Green's function is generally required. In fact, however, we obtain $\mathrm{Im}\bar{G}^R > 0$ for $\Omega > \gamma$ owing to a numerical error. It is seen from Fig. 8 that as long as γ is not very large, $\mathrm{Im}\bar{G}^R$ has a considerably sharp peak. As for the results for $Z = 1$ we can use the relation

$$\mathrm{Im}\bar{G}^R(\Omega,\gamma;1) = \mathrm{Im}\bar{G}^R(-\Omega,\gamma;-1)$$

found from Eq. (2.65).

Now we discuss the impurity scattering effect on the dielectric screening, neglecting the phonon scattering effect which is considered to be small. The general expressions for ϵ_0 and $\epsilon(\vec{q})$ are given through Eq. (2.18). The impurity scattering effect on ϵ_0 can be neglected since ϵ_0 arises from the interband term, i.e., $\chi_{ll'}(l \neq l')$, and the energies

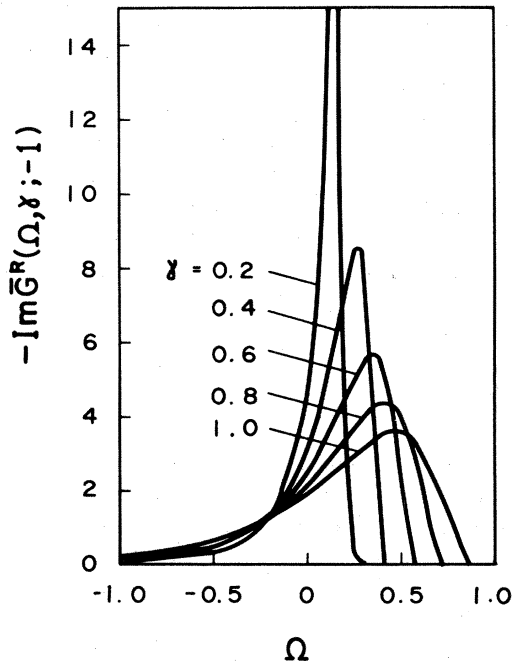

FIG. 8. $\mathrm{Im}\bar{G}^R(\Omega,\gamma;-1)$ as a function of Ω for various values of γ.

relevant to the impurity scattering are much smaller than the band-gap energy. We do not calculate $\chi_{ll'}(l\neq l')$ and use the empirical data of ϵ_0. For the intraband term χ_{ll}, however, we must give a detailed discussion of the impurity scattering effect. Replacing sum over ω_m in Eq. (2.18) by the contour integration[16,18] we obtain after replacement $i\omega\rightarrow\omega$

$$\chi_{ll}(\vec{q},\omega)=-\frac{4}{\pi}\int\frac{d\vec{k}}{(2\pi)^3}[F(\vec{k},\vec{q},\omega)+F(\vec{k},-\vec{q},-\omega)]\,, \tag{3.1}$$

where

$$F(\vec{k},\vec{q},\omega)=\left[\frac{\epsilon_0}{|Z|e^2\lambda}\right]^2\int_{-\infty}^{\infty}d\omega'\mathrm{Im}G^R(l\vec{k},\omega')\mathrm{Im}G^R(l\vec{k}+\vec{q},\omega'+\omega)\Theta(\omega')\,. \tag{3.2}$$

Under the condition that a sufficient number of electrons are within the effective range of an impurity potential, we can use the Thomas-Fermi approximation, which is to take $\chi_{ll}(0,0)$ in place of $\chi_{ll}(\vec{q},0)$ in Eq. (2.17). As shown in Appendix C we find

$$F(\vec{k},0,0)=-\frac{\pi}{4}\frac{\partial}{\partial\xi_{l\vec{k}}}\Theta(\xi_{l\vec{k}})\,, \tag{3.3}$$

so that we obtain Eq. (2.22). Thus we have the usual Thomas-Fermi potential, which is obtained without considering the impurity scattering effect. This result agrees with the fact that we have derived the Green's function under the assumption of a sufficiently slowly varying impurity potential. The criterion for this assumption is $\lambda/n_i^{1/3}<2.6$, as given in Appendix B. On the other hand, the criterion for the Thomas-Fermi approximation is that the number of electrons within the effective range of an impurity potential is large enough, i.e., $n_i/\lambda^3>>1$. Thus both criteria are expressed commonly as $\lambda/n_i^{1/3}<<1$. Further, if $\chi_{ll}(\vec{q},0)$ with $\vec{q}\neq 0$ is used in Eq. (2.17) assuming the free-carrier screening, we obtain the Lindhart potential. This potential is found from numerical calculation to be well approximated by the Thomas-Fermi potential in the range

$$\frac{\lambda}{k_F}\lesssim 1\,, \tag{3.4}$$

where k_F is the magnitude of the wave vector at the Fermi level. Here, degenerate statistics and spherical energy surface for the relevant band are assumed. Taking $|Z|=1$ and noting $k_F=(3\pi^2 n_i)^{1/3}$, Eq. (3.4) offers also the limit of $\lambda/n_i^{1/3}$. Therefore, we may consider the relation (3.4) as a criterion that the present theory of the impurity scattering is justified.

Here, we test directly the validity of the theory of the impurity scattering. We first discuss the conductivity of n-type Ge at 4.2 K, the data[20] of which are available in the high doping range. For such an indirect gap material we consider the CB with v valleys, each of which is assumed to have spherical energy surface. The expression for the dc conductivity tensor $\sigma_{\mu\nu}$ has been given[21] by Bonch-Bruevich. We give this in a form more tractable for this paper in Appendix D. For cubic symmetry we have $\sigma_{\mu\nu}=\Delta(\mu-\nu)\sigma$. We obtain

$$\sigma=-\frac{v}{3\pi^3}\frac{e^2\hbar^3}{m_C^2}\int_0^{\infty}dk\,k^4\int_{-\infty}^{\infty}d\omega\frac{d}{d\omega}\Theta(\omega)\times[\mathrm{Im}G^R(l\vec{k},\omega)]^2\,, \tag{3.5}$$

where m_C is the mass of the CB and l means the CB here. The Fermi level is determined from Eqs. (2.29) and (2.30), taking v valleys into account. We assume singly ionized donors, i.e., $Z=-1$. We consider the temperature to be 0 K as an approximation. The phonon scattering effect is neglected, i.e., $\Sigma_3^R(l\vec{k},\omega)=E_x(l\vec{k})$, in calculating the Green's function. The exchange energy is calculated from Eq. (2.36). The curve of σ^{-1} calculated using $v=4$ and $m_C/m_0=0.12$ for n-Ge, where m_0 is the electron mass in the free space, is shown in Fig. 9 together with the experimental data.[20] We see a considerably good agreement between the theory and the experiments though the theoretical curve lies a little higher than the experimental data. In contrast, the curves that are calculated in Ref. 20 using the earlier theories do not agree with the experiments, as shown in Fig. 9.

Next, we compare the energy density of states $\rho(\omega)$ given by Eq. (2.29) with the data[22] of p-type GaAs at 4.2 K. The calculation is done for 0 K, neglecting again the phonon scattering effect. We use the material parameters shown in Table III, as-

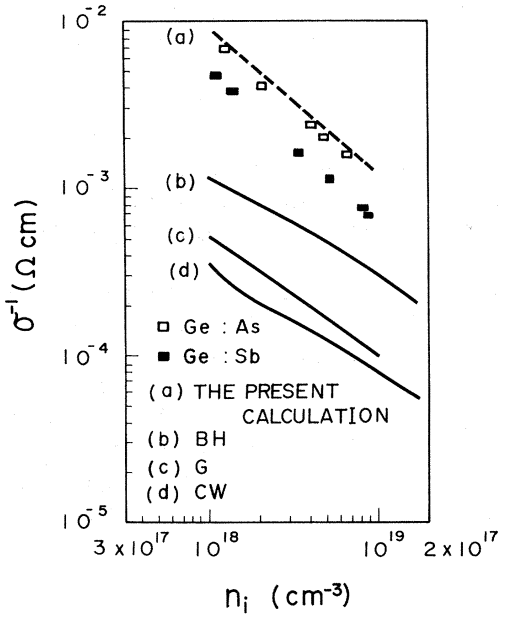

FIG. 9. Resistivity σ^{-1} as a function of donor concentration n_I for n-type Ge. The open and the full rectangles (□ and ■) show the experimental data (Ref. 20). The broken line (a) shows the present calculation. The full lines show the results calculated (Ref. 20) on the basis of the treatment of Brooks-Herring (b), Gulyaev (c), and Conwell-Weiskopf (d).

suming spherical energy surface of the HB with the effective mass m_H. The result of the calculation is shown in Fig. 10 as $a_B^3 E_{F0}\rho(\omega)$, where a_B is the Bohr radius defined as $a_B=\hbar^2\epsilon_0/(m_H e^2)$, and E_{F0} is the Fermi level for a pure crystal measured downward from the HB edge, i.e., $E_{F0}=\hbar^2 k_F^2/(2m_H)$. The experimental data are also plotted in the figure so that experimental value may fit the theoretical one at a certain energy level lying deep in the band. It is seen that the theoretical curve deviates from the experimental values especially in the band-gap region. The reason is that the assumption of the slowly varying impurity potential is not justified there, as discussed in Appendix B. The energy density of states is underestimated thereby. This may be the main reason for the small but significant discrepancy between the present theory and experiments on σ in Fig. 9. For the same reason the Auger recombination rate will be underestimated though the underestimation also may not be very serious.

IV. FORMULAS FOR THE AUGER RECOMBINATION LIFETIME

In this section we discuss the Auger recombination lifetime. Hereafter we restrict the discussion

TABLE III. Material parameters and calculated band parameters.

Parameter	GaAs	InP	GaSb	InAs
E_{G0} (eV)	1.522	1.421	0.8128	0.4105
Δ_{00} (eV)	0.34	0.13	0.743	0.38
E_{G1} (eV K^{-1})	5.8×10^{-4}	2.9×10^{-4}	3.7×10^{-4}	3.35×10^{-4}
Δ_{01} (eV K^{-1})	0	0	1.89×10^{-4}	1.0×10^{-4}
T_0 (K)	300	0	0	248
m_C/m_0[c]	0.067	0.078	0.043	0.023
m_H/m_0	0.45	0.8	0.33	0.41
m_S/m_0[c]	0.11	0.12	0.12	0.083
f_{CH}[c]	5.63	4.76	9.64	18.0
f_{SH}[c]	1.99	1.84	$4.34E_2$[a]	$20.1E_2$[a]
ϵ_0	13.18	12.35	15.69	14.55
$(\epsilon_\infty)^{-1}$	0.0159	0.0055	0.0241	0.0160
c_l(10^{12} dyn/cm^2)	1.397	1.037	1.212	1.030
c_t(10^{12} dyn/cm^2)	0.4862	0.3551	0.3652	0.3136
$\bar{c}$(10^{12} dyn/cm^2)	0.7898	0.5824	0.6407	0.5524
h_{14}(10^4 esu)	4.833	3.167		1.167
P_{pe}	0.0526	0.0403	0.015[b]	0.0156
Ξ (eV)	6.6	6.9	7.0	6.1
E_{npo} (eV)	6.5	5.9	6.3	5.7
ω_{op} (eV)	0.0296	0.0298	0.0394	0.0302

[a] E_2 in eV.
[b] Assumed.
[c] Calculated.

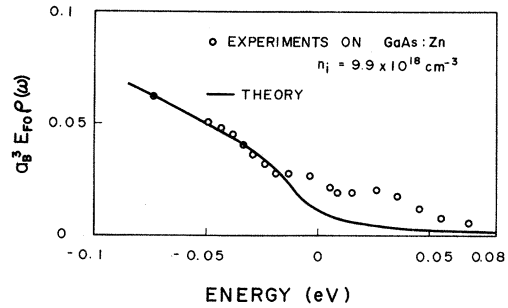

FIG. 10. Energy density of states $\rho(\omega)$ as a function of the energy ω is shown on the present theory (—) and the experiments (Ref. 22) (○).

to direct-gap semiconductors of p-type, which are doped with singly ionized shallow acceptors, i.e., $Z=1$. We consider the Auger process, where a given electron 1 transits down to a hole state 4 exciting another electron 2 to another hole state 3, as shown in Fig. 1. This process is denoted as the 1432 process. Considering the CB, the HB, the light-hole band (LB), and the SB, various transition processes are possible such as CHHS, CHHL, CHHH and so on. Among them, the CHHS process shown in Fig. 1 may be predominant[9,14] in a p-type semiconductor so that only this process is considered. As was done in II, the Auger recombination lifetime τ_{ip} is found from that part of the self-energy $\Sigma^R(l\vec{k},\omega)$, which comes from the electron-electron interaction, i.e., $U_{e\text{-}e}$. This procedure is not repeated here. Assuming infinitesimally small departure from thermal equilibrium, we consider the quasi-Fermi-level F_1 for the minority carriers and that for the majority carriers. From the latter are measured all the energies (including F_1). We have

$$\frac{1}{\tau_{ip}}=\frac{1}{\delta n}\frac{4}{\hbar\pi^3}\int\frac{d\vec{k}_2}{(2\pi)^3}\int\frac{d\vec{k}_3}{(2\pi)^3}\int\frac{d\vec{k}_4}{(2\pi)^3}(|f|^2+|g|^2+|f-g|^2)$$
$$\times\int d\omega_2\int d\omega_3\int d\omega_4 F(\omega_1,\omega_2,\omega_3,\omega_4)\prod_{j=1}^{4}[\mathrm{Im}G^R(l_j\vec{k}_j,\omega_j)]\,, \quad (4.1)$$

where δn is the minority-carrier concentration, $\vec{k}_1=\vec{k}_3+\vec{k}_4-\vec{k}_2$, $\omega_1=\omega_3+\omega_4-\omega_2$,

$$f=\langle l_1\vec{k}_1\,|\,l_4\vec{k}_4\rangle\langle l_2\vec{k}_2\,|\,l_3\vec{k}_3\rangle U_{e\text{-}e}(\vec{k}_4-\vec{k}_1)\,, \quad (4.2)$$

$$g=\langle l_1\vec{k}_1\,|\,l_3\vec{k}_3\rangle\langle l_2\vec{k}_2\,|\,l_4\vec{k}_4\rangle U_{e\text{-}e}(\vec{k}_3-\vec{k}_1)\,, \quad (4.3)$$

and

$$F(\omega_1,\omega_2,\omega_3,\omega_4)=\{\Theta(\omega_2)[1-\Theta(\omega_3)][1-\Theta(\omega_4)]+[1-\Theta(\omega_2)]\Theta(\omega_3)\Theta(\omega_4)\}\Theta(\omega_1-F_1)\,. \quad (4.4)$$

Let us rewrite Eq. (4.1) in a more tractable but approximate form. We know that $\mathrm{Im}\bar{G}^R(l\vec{k},\omega)$ has a maximum at a certain value of $\mathrm{Re}\Omega$, where Ω is given from Eqs. (2.32) and (2.60) as

$$\Omega=\frac{\epsilon_0}{|Z|e^2\lambda}[\omega-\xi_{l\vec{k}}-\Sigma^R_{e\text{-ph}}(l\vec{k},\omega)]\,. \quad (4.5)$$

Here we have rewritten $\xi_{l\vec{k}}+E_x(l\vec{k})$ as $\xi_{l\vec{k}}$, considering this as a renormalized energy. Hereafter, we restrict the discussion to the high doping range where the impurity scattering effect is much larger than the phonon scattering effect. In fact, this condition is satisfied for the impurity concentrations down to 10^{17} cm^{-3}. Then the maximum of $\mathrm{Im}G^R(l\vec{k},\omega)$ is found approximately at $\omega=\xi_{l\vec{k}}+E_0$, where E_0 is $|Z|e^2\lambda/\epsilon_0$ times Ω giving the maximum of $\mathrm{Im}\bar{G}^R(\Omega,\gamma;Z)$. We neglect the phonon-induced energy shift, i.e., $\mathrm{Re}\Sigma^R_{e\text{-ph}}(l\vec{k},\omega)$. This is included in the band-gap energy, of which the empirical value is used. Considering that $\mathrm{Im}\Sigma^R_{e\text{-ph}}(l\vec{k},\omega)$ is proportional to the effective mass of the band l as shown in II, the phonon scattering effects are neglected for the CB and for the SB. Noting that $\mathrm{Im}\Sigma^R_{e\text{-ph}}(l\vec{k},\omega)$ was assumed to be small, we can write

$$\prod_{j=1}^{4}[\mathrm{Im}\bar{G}^R(\Omega_j)]=\mathrm{Im}\bar{G}^R(\Omega_{10})\mathrm{Im}\bar{G}^R(\Omega_{20})[\,\mathrm{Im}\bar{G}^R(\Omega_{30})\mathrm{Im}\bar{G}^R(\Omega_4)+\mathrm{Im}\bar{G}^R(\Omega_3)\mathrm{Im}\bar{G}^R(\Omega_{40})$$
$$-\mathrm{Im}\bar{G}^R(\Omega_{30})\mathrm{Im}\bar{G}^R(\Omega_{40})]\,, \quad (4.6)$$

which is correct up to the first order in $\mathrm{Im}\Sigma^R_{e\text{-ph}}(l\vec{k},\omega)$'s. Here an abbreviation $\bar{G}^R(\Omega_j)=\bar{G}^R(\Omega_j,\gamma;Z)$ is used, where Ω_j is obtained from Eq. (4.5) by the replacement $\omega\to\omega_j$, $l\to l_j$, and $\vec{k}\to\vec{k}_j$. Ω_{j0} is obtained from Ω_j by taking $\mathrm{Im}\Sigma^R_{e\text{-ph}}(l\vec{k}_j,\omega_j)=0$. We use Eq. (4.6) in Eq. (4.1). As seen from Fig. 8, $\mathrm{Im}\bar{G}^R(\Omega)$'s are more rapidly varying functions of ω's than $F(\omega_1,\omega_2,\omega_3,\omega_4)$ and $\mathrm{Im}\Sigma^R_{e\text{-ph}}(l\vec{k},\omega)$'s in Eq. (4.1). We evaluate $F(\omega_1,\omega_2,\omega_3,\omega_4)$ and $\mathrm{Im}\Sigma^R_{e\text{-ph}}(l\vec{k},\omega)$ with $\omega_j=\xi_{l_j\vec{k}_j}+E_0$ where $j=1$, 2, and 3 for the first term of Eq. (4.6), noting $\omega_4=\omega_1+\omega_2-\omega_3=\xi_{l_1\vec{k}_1}+\xi_{l_2\vec{k}_2}-\xi_{l_3\vec{k}_3}+E_0$. For the second term of Eq. (4.6) the evaluation is made with $\omega_j=\xi_{l_j\vec{k}_j}+E_0$ where $j=1$, 2, and 4, noting $\omega_3=\omega_1+\omega_2-\omega_4=\xi_{l_1\vec{k}_1}+\xi_{l_2\vec{k}_2}-\xi_{l_4\vec{k}_4}+E_0$. Since both l_3 and l_4 stand for the HB Eq. (4.1) is the same for replacement $3\to4$ and $4\to3$ of suffices. Noting this and after some manipulation valid up to the first order in $\Sigma^R_{e\text{-ph}}(l\vec{k},\omega)$, we obtain

$$\frac{1}{\tau_{ip}}=\frac{1}{\delta n}\frac{4}{\hbar\pi^3}\left[\frac{\epsilon_0}{e^2\lambda}\right]^4\int\frac{d\vec{k}_2}{(2\pi)^3}\int\frac{d\vec{k}_3}{(2\pi)^3}\int\frac{d\vec{k}_4}{(2\pi)^3}(|f|^2+|g|^2+|f-g|^2)$$
$$\times F(\xi_1+E_0,\xi_2+E_0,\xi_1+\xi_2-\xi_4+E_0,\xi_4+E_0)$$
$$\times H(l_1\vec{k}_1,l_2\vec{k}_2,l_3\vec{k}_3,l_4\vec{k}_4)\,, \tag{4.7}$$

where ξ_j ($j=1,2,3,4$) is an abbreviated notation for $\xi_{l_j\vec{k}_j}$ and

$$H(l_1\vec{k}_1,l_2\vec{k}_2,l_3\vec{k}_3,l_4\vec{k}_4)=\int d\omega_2\int d\omega_3\int d\omega_4\prod_{j=1}^{4}[\mathrm{Im}\bar{G}^R(\Omega_j)]\,. \tag{4.8}$$

Here we define

$$\Omega_3=[\epsilon_0/(e^2\lambda)][\omega_3-\xi_3-2\,\mathrm{Im}\Sigma^R_{e\text{-ph}}(l_3\vec{k}_3,\xi_1+\xi_2-\xi_4+E_0)]$$

and

$$\Omega_j=[\epsilon_0/(e^2\lambda)](\omega_j-\xi_j)$$

for $j=1$, 2, and 4. We define also $\vec{k}_1=\vec{k}_3+\vec{k}_4-\vec{k}_2$ and $\omega_1=\omega_3+\omega_4-\omega_2$.

The integration over ω's in Eq. (4.8) is performed using Eq. (2.64) and noting the relation

$$\int_{-\infty}^{\infty}d\omega\cos\left[\frac{\epsilon_0}{e^2\lambda}(\xi_1-\xi_2)\omega\right]=\frac{\pi e^2\lambda}{\epsilon_0}\delta(\xi_1-\xi_2)\,. \tag{4.9}$$

We obtain

$$H(l_1\vec{k}_1,l_2\vec{k}_2,l_3\vec{k}_3,l_4\vec{k}_4)=\left[\frac{\pi e^2\lambda}{\epsilon_0}\right]^3U(\Omega_r,\Omega_i;\gamma)\,, \tag{4.10}$$

where we define

$$U(\Omega_r,\Omega_i,\gamma)=\int_0^\infty d\xi\cos(\xi\Omega_r)\times\exp[4\gamma g_r(\xi)-2\xi\Omega_i]\,, \tag{4.11}$$

$$\Omega_r=\frac{\epsilon_0}{e^2\lambda}(\xi_1+\xi_2-\xi_3-\xi_4)\,, \tag{4.12}$$

$$\Omega_i=-\frac{\epsilon_0}{e^2\lambda}\mathrm{Im}\Sigma^R_{e\text{-ph}}(l_3\vec{k}_3,\xi_1+\xi_2-\xi_4+E_0)\,, \tag{4.13}$$

and $g_r(\xi)$ is the real part of $g(\xi)$, i.e.,

$$g_r(\xi)=\int_0^\infty dx\,x^2\left[\cos\left[\frac{\xi}{x}\exp(-x)\right]-1\right]. \tag{4.14}$$

An approximate form of F in Eq. (4.4) is given here. Let us assume that the spin splitoff energy Δ_0 is far larger than the thermal energy T. Then the SB is almost completely full of electrons so that we obtain $\Theta(\omega_2)=1$ as a good approximation. Further, since we consider infinitesimally small concentrations of the minority carriers, nondegenerate statistics is applied to $\Theta(\omega_1-F_1)$. We obtain

$$F(\omega_1,\omega_2,\omega_3,\omega_4)=\frac{1}{\exp\left[\frac{\omega_3}{T}\right]+1}\,\frac{1}{\exp\left[\frac{\omega_4}{T}\right]+1}\times\exp\left[\frac{F_1+\omega_2}{T}\right]. \tag{4.15}$$

Now formulas for finding the quasi-Fermi-levels

are given in tractable forms using Eqs. (2.29) and (2.30). As for the majority carriers we evaluate $\Theta'(\omega)$ approximately with $\omega=\xi_{H\vec{k}}+E_0$ giving a maximum of $\mathrm{Im}G^R$, where $\xi_{H\vec{k}}$ is the energy for the HB. Then the integration over ω is performed noting the relation similar to Eq. (4.9). We replace $\xi_1-\xi_2$ by ξ so that π in the right-hand side is replaced by $\pi/2$. We obtain

$$n_i=2\int\frac{d\vec{k}}{(2\pi)^3}[1-\Theta(\xi_{H\vec{k}}+E_0)]\,. \tag{4.16}$$

Similarly we have

$$\delta n=2\int\frac{d\vec{k}}{(2\pi)^3}\exp[(F_1-\xi_{C\vec{k}}-E_0)/T]\,, \tag{4.17}$$

with $\xi_{C\vec{k}}$ being the energy for the CB.

Here, we assume spherical energy surfaces for the CB, HB, and SB, defining the effective masses m_C, m_H, and m_S, respectively, for those bands. The energies measured from the respective band edges upward (CB) or downward (HB and SB) are given by $\hbar^2k^2/2m_l$ with $l=C$, H, and S. In general, m_l depends on $\vec{k}$. Let us recall that ω and $\xi_{l\vec{k}}$ are measured from the Fermi level for the majority carriers. We have $\xi_1=E_1+E_G+F_p$, $\xi_2=-\Delta_0-E_2+F_p$, $\xi_3=-E_3+F_p$, and $\xi_4=-E_4+F_p$, where E_G is the band-gap energy, F_p the quasi-Fermi-level for the majority carriers measured downward from the HB edge, $E_1=\hbar^2k_1^2/(2m_C)$, $E_2=\hbar^2k_2^2/(2m_S)$, $E_3=\hbar^2k_3^2/(2m_H)$, and $E_4=\hbar^2k_4^2/(2m_H)$. Using m_H at $\vec{k}=0$, Eq. (4.16) is rewritten as

$$n_i=\frac{2}{\sqrt{\pi}}N_VF_{1/2}(\eta_p)\,, \tag{4.18}$$

where $\eta_p=(F_p+E_0)/T$,

$$N_V=2\left[\frac{m_HT}{2\pi\hbar^2}\right]^{3/2} \tag{4.19}$$

is the effective density of the states for the valence band, and $F_{1/2}(\eta_p)$ is defined through the Fermi integral

$$F_a(b)=\int_0^\infty dx\frac{x^a}{\exp(x-b)+1}\,. \tag{4.20}$$

Using m_C at $\vec{k}=0$ Eq. (4.17) is rewritten as

$$\delta n=N_C\exp\left[\frac{F_1-E_G-F_p-E_0}{T}\right], \tag{4.21}$$

where N_C is the effective density of states for the CB,

$$N_C=2\left[\frac{m_CT}{2\pi\hbar^2}\right]^{3/2}. \tag{4.22}$$

Using Eqs. (4.10)–(4.22), Eq. (4.7) is rewritten as

$$\frac{1}{\tau_{ip}}=\frac{4}{\hbar}\frac{1}{N_C}\frac{\epsilon_0}{e^2\lambda}\exp\left[2\eta_p+\frac{E_G-\Delta_0}{T}\right]\times\int\frac{d\vec{k}_2}{(2\pi)^3}\int\frac{d\vec{k}_3}{(2\pi)^3}\int\frac{d\vec{k}_4}{(2\pi)^3}\exp\left[-\frac{E_2}{T}\right]\frac{1}{\exp\left[\eta_p+\dfrac{E_1-E_2+E_4+E_G-\Delta_0}{T}\right]+1}\times\frac{1}{\exp\left[\eta_p-\dfrac{E_4}{T}\right]+1}U(\Omega_r,\Omega_i;\gamma)(|f|^2+|g|^2+|f-g|^2)\,, \tag{4.23}$$

where

$$\Omega_r=\frac{\epsilon_0}{e^2\lambda}(E_1-E_2+E_3+E_4+E_G-\Delta_0)\,, \tag{4.24}$$

and

$$\Omega_i=-\frac{\epsilon_0}{e^2\lambda}\mathrm{Im}\Sigma^R_{e\text{-ph}}(l_3\vec{k}_3,E_1-E_2+E_4+E_G-\Delta_0+E_0+F_p)\,. \tag{4.25}$$

This is the central result of this paper.

Especially when the impurity and phonon scattering effects are neglected, we obtain the pure collision Auger recombination. The neglect of both effects corresponds to replacing $4\gamma g_r(\xi)-2\xi\Omega_i$ in Eq. (4.11) by $-\xi\delta$ so that we obtain $U=\pi\delta(\Omega_r)$. The lifetime of the pure collision Auger recombination τ_0 is given by

$$\frac{1}{\tau_0}=\frac{4\pi}{\hbar}\frac{1}{N_C}\exp\left[2\eta_p+\frac{E_G-\Delta_0}{T}\right]$$
$$\times\int\frac{d\vec{k}_2}{(2\pi)^3}\int\frac{d\vec{k}_3}{(2\pi)^3}\int\frac{d\vec{k}_4}{(2\pi)^3}\exp\left[-\frac{E_2}{T}\right]\frac{1}{\exp\left[\eta_p+\frac{E_1-E_2+E_4+E_G-\Delta_0}{T}\right]+1}$$
$$\times\frac{1}{\exp\left[\eta_p-\frac{E_4}{T}\right]+1}\delta(E_1-E_2+E_3+E_4+E_G-\Delta_0)$$
$$\times(|f|^2+|g|^2|f-g|^2)\,. \tag{4.26}$$

The energy conservation requirement implied by the δ function and the momentum conservation $\vec{k}_1=\vec{k}_3+\vec{k}_4-\vec{k}_2$ implicit in the equation gives rise to nonzero threshold energy for the Auger process. On the other hand the impurity and phonon scattering effects, which are present in actual cases, relaxes the above conservation requirements so that the threshold energy is zero. Thus the Auger recombination process is enhanced.

Equation (4.23) has been derived for the case where the impurity scattering effect is predominant though the phonon scattering effect cannot be neglected. On the other hand, the phonon-assisted Auger recombination was discussed in II, where the impurity scattering effect was completely neglected. Considering that the phonon scattering is weak, the lifetime of that process $\tau_{\rm ph}$ is given in II by

$$\frac{1}{\tau_{\rm ph}}+\frac{1}{\tau_0}=\frac{8}{\hbar}\frac{1}{N_C}\exp\left(2\eta_p+\frac{E_G-\Delta_0}{T}\right)$$
$$\times\int\frac{d\vec{k}_2}{(2\pi)^3}\int\frac{d\vec{k}_3}{(2\pi)^3}\int\frac{d\vec{k}_4}{(2\pi)^3}\exp\left[-\frac{E_2}{T}\right]\frac{1}{\exp\left[\eta_p+\frac{E_1-E_2+E_4+E_G-\Delta_0}{T}\right]+1}$$
$$\times\frac{1}{\exp\left[\eta_p-\frac{E_4}{T}\right]+1}\frac{\epsilon_0}{e^2\lambda}\frac{\Omega_i}{\Omega_r^2+\Omega_i^2}(|f|^2+|g|^2+|f-g|^2) \tag{4.27}$$

where we take $E_0=0$. It is seen from Eqs. (4.24) and (4.25) that $[\epsilon_0/(e^2\lambda)]\Omega_i/(\Omega_r^2+\Omega_i^2)$ is independent of $\epsilon_0/(e^2\lambda)$.

Let us give here $(|f|^2+|g|^2+|f-g|^2)$ and Ω_i, which have appeared above. We take the former approximately[2] as $(|f|^2+|g|^2)$. As for the overlap integral we use the relation[23]

$$|\langle l_m\vec{k}_m\,|\,l_n\vec{k}_n\rangle|^2=\frac{\hbar^2}{2m_0}\frac{|\vec{k}_m-\vec{k}_n|^2}{|\xi_{l_m\vec{k}_m}-\xi_{l_n\vec{k}_n}|}f_{mn} \tag{4.28}$$

for the interband matrix, where m_0 and f_{mn} are the electron mass in the free space and the oscillator strength, respectively. We make an approximation $|\xi_{l_m\vec{k}_m}-\xi_{l_n\vec{k}_n}|=E_G$. From Eqs. (4.2) and (4.3) we obtain

$$|f|^2+|g|^2=\left[\frac{2\pi e^2\hbar^2}{m_0\epsilon_0E_G}\right]^2 f_{CH}f_{SH}\left[\left[\frac{|\vec{k}_3-\vec{k}_2|^2}{|\vec{k}_3-\vec{k}_2|^2+\lambda^2}\right]^2+\left[\frac{|\vec{k}_4-\vec{k}_2|^2}{|\vec{k}_4-\vec{k}_2|^2+\lambda^2}\right]^2\right]. \tag{4.29}$$

Ω_i is obtained from Eq. (4.25) using the relations in II as follows:

$$\mathrm{Im}\Sigma^R_{e\text{-ph}}(l_3\vec{k}_3,E_1-E_2+E_4+E_G-\Delta_0+E_0+F_p)=-\frac{2m_H}{\hbar^2}\frac{1}{k_3}[AH_1(k_3,k_0)+BH_2(k_3,k_0)]\,, \tag{4.30}$$

where

$$k_0=\left[\frac{2m_H}{\hbar^2}(E_2-E_1-E_4-E_G+\Delta_0-E_0)\right]^{1/2}, \tag{4.31}$$

$$A=\frac{1}{8\pi}\left[\frac{1}{c_l}\Xi^2T+\frac{1}{2\bar{c}}E^2_{\mathrm{npo}}\omega_{\mathrm{op}}[1+2P(\omega_{\mathrm{op}})]\right], \tag{4.32}$$

$$B=\frac{1}{8\pi}\left[e^2P^2_{pe}T+\frac{2\pi e^2}{\epsilon^*}\omega_{\mathrm{op}}[1+2P(\omega_{\mathrm{op}})]\right], \tag{4.33}$$

$$H_1(k_3,k_0)=2k_0k_3-\lambda^2\left[\ln\left|\frac{(k_3+k_0)^2+\lambda^2}{(k_3-k_0)^2+\lambda^2}\right|-\tfrac{1}{2}\lambda^2\left[\frac{1}{(k_3-k_0)^2+\lambda^2}-\frac{1}{(k_3+k_0)^2+\lambda^2}\right]\right], \tag{4.34}$$

$$H_2(k_3,k_0)=\tfrac{1}{2}\left[\ln\left|\frac{(k_3+k_0)^2+\lambda^2}{(k_3-k_0)^2+\lambda^2}\right|-\lambda^2\left[\frac{1}{(k_3-k_0)^2+\lambda^2}-\frac{1}{(k_3+k_0)^2+\lambda^2}\right]\right]. \tag{4.35}$$

As for Eqs. (4.31) the restrictive condition is that k_0 should be real.

Let us facilitate numerical calculation of τ_{ip} given by Eq. (4.23), starting from discussion of $U(\Omega_r,\Omega_i;\gamma)$ given by Eq. (4.11). If $|\Omega_r|$ is sufficiently large, we obtain approximately

$$U(\Omega_r,\Omega_i;\gamma)=\int_0^\infty d\xi(1-\gamma\xi^2)\cos(\xi\Omega_r)\exp(-2\xi\Omega_i)=\frac{2\Omega_i}{\Omega_r^2+4\Omega_i^2}\left[1+2\gamma\frac{3\Omega_r^2-4\Omega_i^2}{(\Omega_r^2+4\Omega_i^2)^2}\right] \tag{4.36}$$

by the method of the stationary phase, noting that $g_r(\xi)=-\frac{1}{4}\xi^2$ when $\xi\to0$. The equation offers a good approximation if the second term in large parentheses is much smaller than unity. Considering $|\Omega_r|>>\Omega_i$, Eq. (4.36) is found to be useful in the range $\Omega_r^2\gtrsim6\gamma$. On the other hand, if γ is sufficiently large, we obtain approximately

$$\begin{aligned}U(\Omega_r,\Omega_i;\gamma)&=\int_0^\infty d\xi(1-2\xi\Omega_i)\cos(\xi\Omega_r)\exp[4\gamma g_r(\xi)]\\&=U(\Omega_r,0;\gamma)-2\Omega_i\frac{\partial}{\partial\Omega_r}\int_0^\infty d\xi\sin(\xi\Omega_r)\exp[4\gamma g_r(\xi)]\,.\end{aligned}$$

Numerical calculation shows that the left-hand side of

$$\int_0^\infty d\xi\sin(\xi\Omega_r)\exp[4\gamma g_r(\xi)]=\frac{\Omega_r}{\Omega_r^2+\Gamma_s^2} \tag{4.37}$$

is well aproximated by the right-hand side of the equation using

$$\Gamma_s^2=0.948\gamma^{1.8} \tag{4.38}$$

in the range $0.1\lesssim\gamma\lesssim1$. We obtain

$$U(\Omega_r,\Omega_i;\gamma)=U(\Omega_r,0;\gamma)+2\Omega_i\frac{\Omega_r^2-\Gamma_s^2}{(\Omega_r^2+\Gamma_s^2)^2}\,. \tag{4.39}$$

If $|\Omega_r|$ is sufficiently large, $U(\Omega_r,0;\gamma)$ is found to be approximately given by

$$U(\Omega_r,0;\gamma)=\left[\frac{\pi}{4\gamma}\right]^{1/2}\exp\left[-\frac{\Omega_r^2}{4\gamma}\right]. \tag{4.40}$$

From this we see that Eq. (4.39) is not useful when $|\Omega_r|$ is too large. It is found that Eq. (4.39) is useful in the range $\Omega_r^2\lesssim6\gamma$. Therefore we use Eqs. (4.36) and (4.39) for $\Omega_r^2>6\gamma$ and for $\Omega_r^2\lesssim6\gamma$, respectively. As for $U(\Omega_r,0;\gamma)$, we use Eq. (4.40) if $|\Omega_r|$ is large enough and numerically calculate it if $|\Omega_r|$ is small.

A next step to facilitate numerical calculation is to modify Eq. (4.29). Especially at moderate doping levels we can take

$$|\vec{k}_3-\vec{k}_2|^2/(|\vec{k}_3-\vec{k}_2|^2+\lambda^2)=1$$

and

$$|\vec{k}_4-\vec{k}_1|^2/(|\vec{k}_4-\vec{k}_1|^2+\lambda^2)=1 ,$$

as was done before.[23] However this is not a good approximation at high doping levels. We approximately evaluate $|f|^2+|g|^2$ by taking an angular average with respect to the direction of $\vec{k}_2$. In place of Eq. (4.29) we give

$$|f|^2+|g|^2=[(2\pi e^2\hbar^2)/(m_0\epsilon_0 E_G)]^2 \times f_{CH}f_{SH}(\Phi_3+\Phi_4)$$

where $\Phi_j (j=3,4)$ is given by

$$\Phi_j=1+\frac{\lambda^4}{(k_j^2+k_2^2+\lambda^2)^2-4k_j^2k_2^2} -\frac{\lambda^2}{2k_jk_2}\ln\left|\frac{(k_j+k_2)^2+\lambda^2}{(k_j-k_2)^2+\lambda^2}\right| . \quad (4.41)$$

To perform the integration of Eq. (4.23), it is convenient to replace $\int d\vec{k}_2\int d\vec{k}_3\int d\vec{k}_4\cdots$ by $\int d\vec{k}_2\int d\vec{k}_1\int d\vec{k}_4\cdots$ under $\vec{k}_3=\vec{k}_1+\vec{k}_2-\vec{k}_4$ and to give new definitions as follows:

$$z_0=\frac{E_G-\Delta_0}{T} , \quad z_1=\tfrac{1}{2}(z_0+|z_0|) ,$$
$$z+z_1=\frac{E_2}{T} , \quad x=\left[\frac{E_1}{T}\right]^{1/2} , \quad y=\left[\frac{E_4}{T}\right]^{1/2} , \quad (4.42)$$
$$r_0=\sqrt{z+z_1-z_0} , \quad \xi_\lambda=\frac{e^2\lambda}{\epsilon_0 T} .$$

The definition of z_1 is done in view of the cases $E_G<\Delta_0$ as well as $E_G>\Delta_0$. The condition that k_0 in Eq. (4.31) should be real leads to inequality $x^2+y^2\le r_0^2$ under the requirement that r_0 is real. We further define

$$x=r\phi , \quad y=r(1-\phi^2)^{1/2} ,$$
$$\vec{k}_2\cdot\vec{k}_4=k_2k_4\phi_1 , \quad (4.43)$$
$$\vec{k}_1\cdot(\vec{k}_2-\vec{k}_4)=k_1|\vec{k}_2-\vec{k}_4|\phi_2 .$$

We give m_C, m_H, and f_{CH} by the band-edge values, while m_S and f_{SH} are evaluated at $z=z_0$ if $z_0>>1$. If $-\infty<z_0\lesssim 1$, m_S is given at $z=0$ and f_{SH} is given by $f_{SH}=f'_{SH}E_2$ with $f'_{SH}=df_{SH}/dE_2$ at $E_2=0$. We finally obtain

$$\frac{1}{\tau_{ip}}=\frac{8(m_Hm_S)^{3/2}T^2e^4}{\pi^{5/2}\hbar^3m_0^2\epsilon_0^2E_G^2}\frac{f_{CH}}{\xi_\lambda}\exp(2\eta_p+z_0-z_1) \times\int_{-z_1}^{\infty}dz\sqrt{z+z_1}\exp(-z)f_{SH}S(z) , \quad (4.44)$$

where

$$S(z)=\int_0^\infty dr\,r^5\int_0^1 d\phi\,\phi^2(1-\phi^2)^{1/2}\int_{-1}^1 d\phi_1\int_{-1}^1 d\phi_2\frac{1}{\exp(\eta_p+r^2-r_0^2)+1}\frac{1}{\exp(\eta_p-y^2)+1} \times U(\Omega_r,\Omega_i,\gamma)(\Phi_3+\Phi_4) . \quad (4.45)$$

Here Ω_r, Ω_i, Φ_3, and Φ_4 given by Eqs. (4.12), (4.13), and (4.41), should be rewritten using the above new definitions though not shown. It should be noted that we use $U(\Omega_r,\Omega_i;\gamma)$ for $r\le r_0$ if r_0 is real while we use $U(\Omega_r,0;\gamma)$ for $r>r_0$ if r_0 is real or for $r>0$ if r_0 is not real. Using Fig. 8 and Eq. (2.65) E_0 is found to be well simulated by the function

$$E_0=-\frac{e^2\lambda}{\epsilon_0}\frac{\gamma}{0.996+0.877\sqrt{\gamma}} \quad (4.46)$$

in the range $0.1\lesssim\gamma\lesssim 1$. In actual calculations E_0 in k_0 [Eq. (4.31)] is neglected since E_0 is small in the range where the phonon scattering effect is important.

In a similar way the integration of Eq. (4.27) is performed, as described in II. As for the integration of Eq. (4.26), it is convenient to start from a new definition as follows:

$$\vec{j}=\vec{k}_3+\vec{k}_4-b\vec{k}_2 , \quad \vec{h}=\vec{k}_3-\vec{k}_4 , \quad \vec{k}_2=\vec{k}_2 , \quad b=\frac{1}{1+\frac{m_C}{2m_H}} , \quad a=\frac{m_C}{m_S}-1+b ,$$
$$x=\left[\frac{\hbar^2}{2m_Sabt}j^2\right]^{1/2} , \quad y=\left[\frac{m_C}{m_H}\frac{\hbar^2}{4m_SaT}|\vec{h}|^2\right]^{1/2} , \quad x=r\phi , \quad y=r(1-\phi^2)^{1/2} , \quad (4.47)$$
$$\vec{j}\cdot\vec{k}_2=jk_2\phi_1 , \quad \vec{h}\cdot(\vec{j}-b\vec{k}_2)=|\vec{h}||\vec{j}-b\vec{k}_2|\phi_2 .$$

we obtain

$$\frac{1}{\tau_0}=\frac{\sqrt{2}m_S^{7/2}m_H^{3/2}a^2b^{3/2}T^2e^4}{\pi^{3/2}\hbar^3m_C^2m_0^2\epsilon_0^2E_G^2}f_{CH}\exp(2\eta_p+z_0-z_1)$$
$$\times\int_0^\infty dz\sqrt{z+z_1}\left[z+z_1-\frac{m_C}{am_S}z_0\right]^4\exp(-z)f_{SH}S_0(z)\ , \tag{4.48}$$

where

$$S_0(z)=\int_0^1 d\phi\,\phi^2(1-\phi^2)^{1/2}\int_{-1}^1 d\phi_1\int_{-1}^1 d\phi_2\frac{1}{\exp(\eta_p-\eta_3)+1}\frac{1}{\exp(\eta_p-\eta_4)+1}(\Phi_3+\Phi_4)\ . \tag{4.49}$$

Here z_0 and z_1 have been given by the definitions (4.42). η_p is calculated from Eq. (4.18). Φ_3, Φ_4, $\eta_3=E_3/T$, and $\eta_4=E_4/T$ are given using the definitions (4.47).

Let us discuss the approximation that we have taken $\omega=\xi_{l\vec{k}}+E_0$ in Eqs. (4.15)–(4.17). This results in overestimation and underestimation of the relevent integrations for the CB and for the HB, respectively, as long as E_0 is calculated from Eq. (4.46). On the other hand, we find that E_0 appears in the forms of $F_1-F_p-E_0$ and F_p+E_0 in all the relevant equations except Eq. (4.31). In place of using Eq. (4.46) we give E_0 two different values for the CB and for the HB so that F_1 and F_p, which are approximately calculated from Eqs. (4.18) and (4.21), may be correct values, which are directly calculated from Eqs. (2.29) and (2.30). In this way the overestimation and the underestimation are reduced. Actually, this is automatically done only by using Eqs. (4.18) and (4.21) since we are not interested in the values of F_1, F_p, and E_0 separately.

V. RESULTS AND DISCUSSIONS

The theory in the previous sections is applied to the p-type materials of GaAs, InP, GaSb, and InAs, which are doped with singly ionized shallow acceptors. For the former two materials we have $E_G>>\Delta_0$ and for the latter two we have $E_G\simeq\Delta_0$. We give the temperature-dependent E_G and Δ_0 as

$$E_G=E_{G0}-E_{G1}T^2/(T+T_0) \tag{5.1}$$

and

$$\Delta_0=\Delta_{00}+\Delta_{01}T\ , \tag{5.2}$$

where E_G, E_{G0}, Δ_0, and Δ_{00} are in eV, E_{G1}, and Δ_{01} in eV K^{-1}, and T in K. The band parameters to be used are calculated on the basis of the $\vec{k}\cdot\vec{p}$ perturbation theory[24] using the numerical values of the interband matrix elements given by Lawaetz.[25]. The material parameters[26] and the calculated band parameters are shown in Table III. In order to calculate τ_{ip} from Eqs. (4.44) and (4.45), computation of $S(z)$ using Weyl's Gleichverteilung method followed by numerical integration over z was performed. For $E_G>\Delta_0$ the range of the integration over r is divided into two zones $0\le r<r_0$ and $r_0\le r\le r_\infty$, where r_∞ is an adequate upper value. For $E_G<\Delta_0$ a single zone $0\le r\le r_\infty$ is used. At most, 200 combinations of $(\gamma,\phi,\phi_1,\phi_2)$ with random values were found to yield well convergent results. The lifetimes of the pure collision Auger recombination τ_0 and the phonon-assisted Auger recombination $\tau_{\rm ph}$ were calculated by the same procedure. It is convenient to present the results in terms of Auger coefficients $\pi^{-1}C_{ip}$, $\pi^{-1}C_0$, and $\pi^{-1}C_{\rm ph}$ defined through $\tau_{ip}^{-1}=\pi^{-1}C_{ip}n_i^2$, $\tau_0^{-1}=\pi^{-1}C_0n_i^2$, and $\tau_{\rm ph}^{-1}=\pi^{-1}C_{\rm ph}n_i^2$. We calculated C_{ip} and C_0 for $n_i=10^{17}$, 10^{18}, 10^{19}, and 10^{20} cm^{-3}. Then curves for the Auger coefficients were obtained by interpolation.

The results for C_{ip}, C_0, and $C_{\rm ph}$ are shown in Figs. 11–14, 15–18, and 19, respectively. In the case of GaAs and InP the Auger recombination is remarkably enhanced by the impurity and phonon scattering as compared with the pure collision Auger recombination especially at low temperatures and/or at light-doping levels. The range where appreciable enhancement is found is of $n_i\lesssim10^{19}$ cm^{-3} and/or of $T\lesssim300$ K. Outside the range C_{ip} can be roughly approximated by C_0. In the case of GaSb and InAs, on the other hand, C_{ip} is close to C_0 over all the range of n_i and T considered. The reason why C_{ip} is more or less close to C_0 in the above cases is as follows. The enhancement of the Auger recombination is caused by reducing the threshold energy for the pure collision Auger recombination to zero. However, the

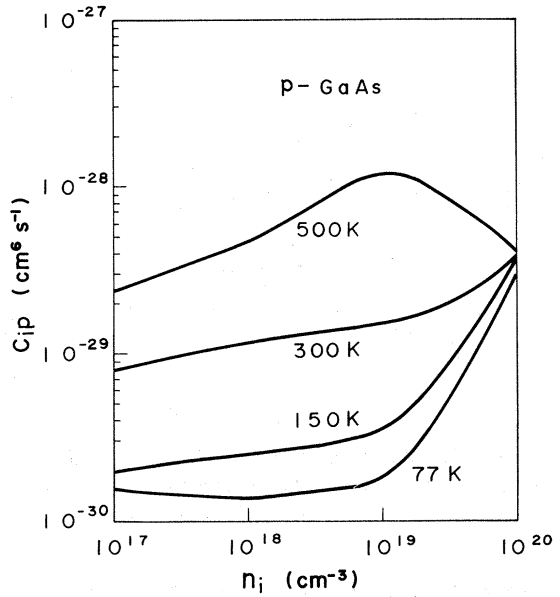

FIG. 11. Auger coefficient of the impurity- and phonon-assisted recombination $\pi^{-1}C_{ip}$ on GaAs as a function of the acceptor concentration n_i for various temperatures.

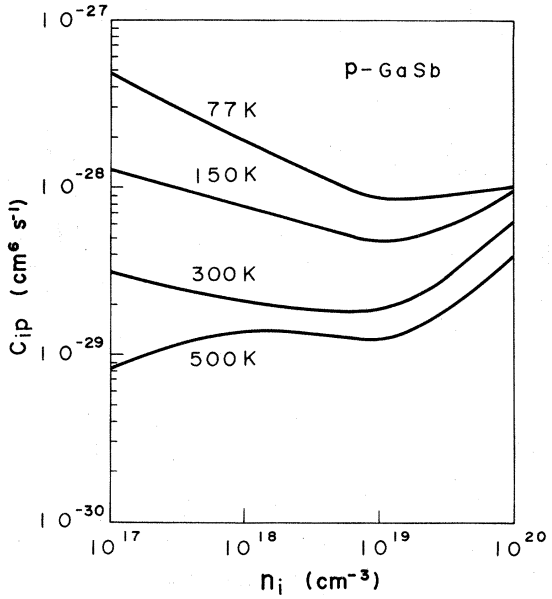

FIG. 13. Auger coefficient of the impurity- and phonon-assisted recombination $\pi^{-1}C_{ip}$ on GaSb as a function of the acceptor concentration n_i for various temperatures.

Auger recombination is little influenced by the presence of the threshold energy as long as the temperature is high enough and/or the degenerate statistics are applicable to the majority carriers. Especially if $E_G \simeq \Delta_0$ such as in GaSb and InAs, the threshold energy is almost or absolutely zero. Therefore in those cases the Auger recombination is little influenced by the impurity and phonon scattering. It is to be noted here that we have $C_{ip} \simeq C_0$ for n_i down to 10^{17} cm^{-3} in GaSb and InAs. This indicates that the present theory is well applicable in the range of $n_i \gtrsim 10^{17}$ cm^{-3} though this is only roughly guaranteed by the criterion (3.8).

In Fig. 19 the Auger coefficient $\pi^{-1}C_{\rm ph}$ which is calculated assuming the phonon-assisted process alone is shown. The results are shown only for the case of $n_i = 10^{17}$ cm^{-3}. It was shown in II that

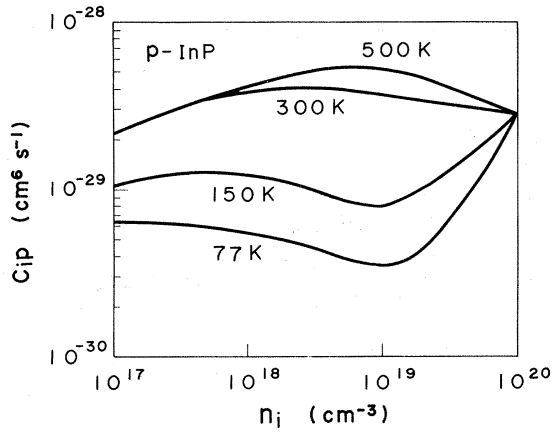

FIG. 12. Auger coefficient of the impurity- and phonon-assisted recombination $\pi^{-1}C_{ip}$ on InP as a function of the acceptor concentration n_i for various temperatures.

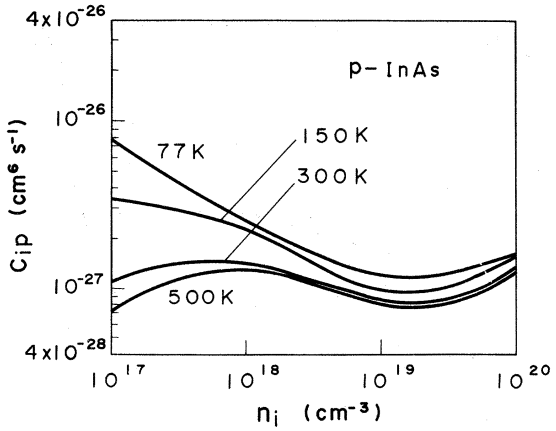

FIG. 14. Auger coefficient of the impurity- and phonon-assisted recombination $\pi^{-1}C_{ip}$ on InAs as a function of the acceptor concentration n_i for various temperatures.

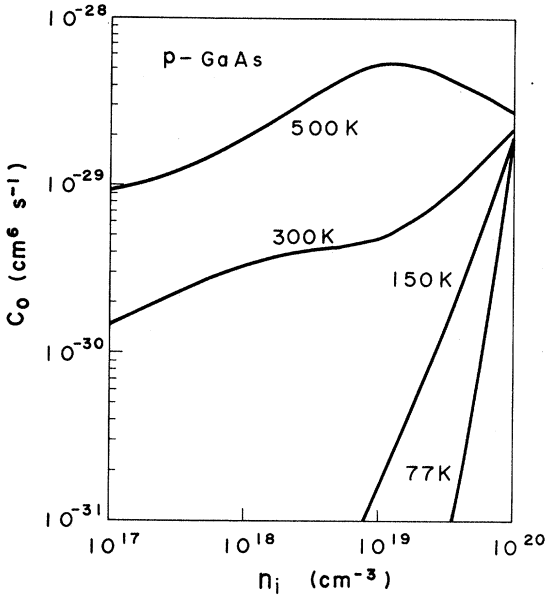

FIG. 15. Auger coefficient of the pure collision recombination $\pi^{-1}C_0$ on GaAs as a function of the acceptor concentration n_i for various temperatures.

$C_{\rm ph}$ is nearly independent of n_i in the range of $n_i \lesssim 10^{19}$ cm^{-3}. Comparison of C_{ip} with $C_{\rm ph}$ shows that the Auger recombination is suppressed by the impurity scattering for GaSb and InAs while C_{ip} is close to $C_{\rm ph}$ for GaAs and InAs. The reason for the suppression is that the band states

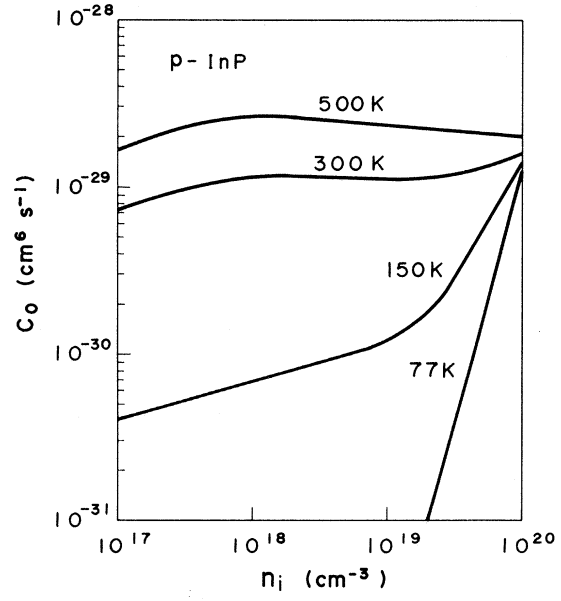

FIG. 16. Auger coefficient of the pure collision recombination $\pi^{-1}C_0$ on InP as a function of the acceptor concentration n_i for various temperatures.

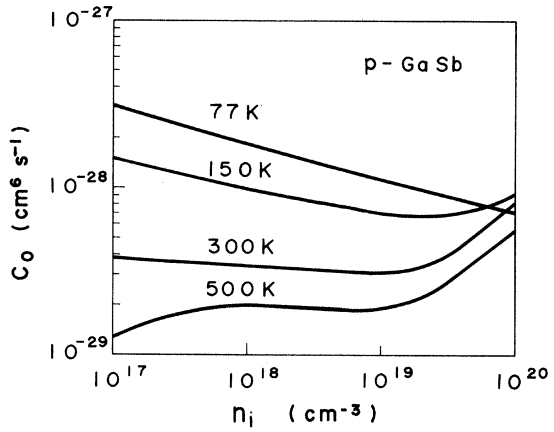

FIG. 17. Auger coefficient of the pure collision recombination $\pi^{-1}C_0$ on GaSb as a function of the acceptor concentration n_i for various temperatures.

are broadened by the impurity scattering to a degree beyond that which is efficient in increasing the state density around the band edges.

Now comparison of the theory with experiments[7] is made on p-type GaAs and p-type InAs with $n_i = 10^{19}$ cm^{-3} at 77 K. The experimental value of the Auger coefficient for GaAs is $10^{-(31\pm1)}$ cm^{6}s^{-1}, while the theory gives $\pi^{-1}C_{ip} = 0.51 \times 10^{-30}$ cm^{6}s^{-1} in considerably good agreement. On the other hand, the experimental value for GaSb is $10^{-(25\pm1)}$ cm^{6}s^{-1}, which does not agree with the theoretical value, $\pi^{-1}C_{ip} = 3.0 \times 10^{-29}$ cm^{6}s^{-1}. Even the theoretical value $\pi^{-1}C_{\rm ph} = 0.38 \times 10^{-27}$ cm^{6}s^{-1} is much smaller than the experimental one. The discrepancy cannot be explained within the framework of the present theory.

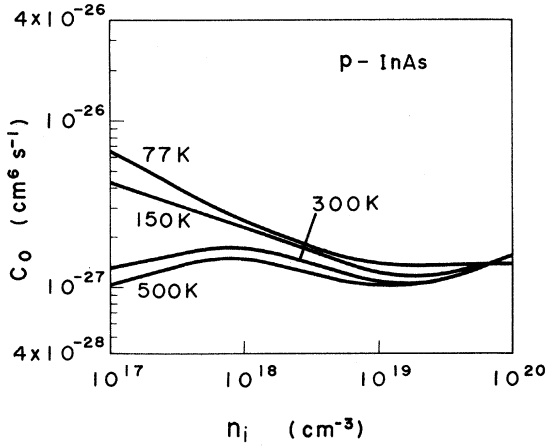

FIG. 18. Auger coefficient of the pure collision recombination $\pi^{-1}C_0$ on InAs as a function of the acceptor concentration n_i for various temperatures.

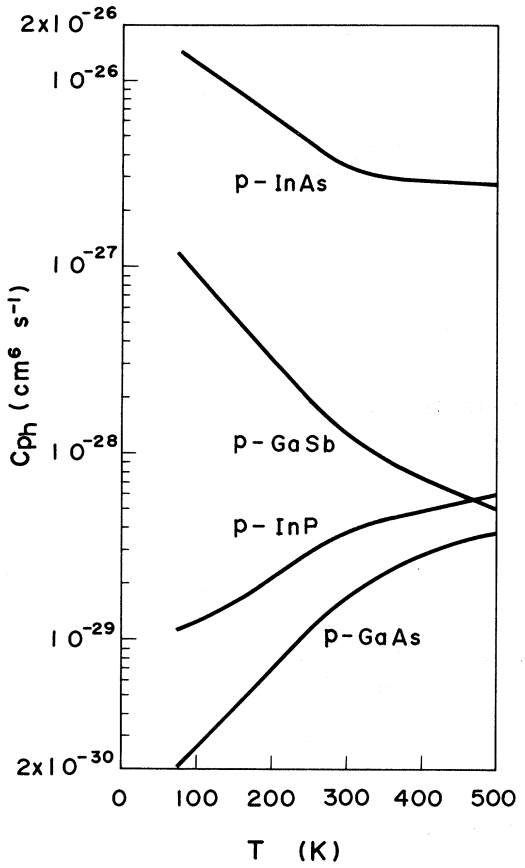

FIG. 19. Auger coefficient of the phonon-assisted recombination $\pi^{-1}C_{\rm ph}$ on GaAs, InP, GaSb, and InAs, as a function of the temperature for the acceptor concentration of 10^{17} cm^{-3}.

A conclusion for direct gap materials of p-type is as follows.

(i) At light doping levels ($n_i \lesssim 10^{17}$ cm^{-3}) the phonon-assisted Auger recombination is predominant for all materials.

(ii) For materials with E_G larger than Δ_0 plus several times the thermal energy T the impurity- and phonon-assisted Auger recombination is predominant in the range of 10^{17} cm$^{-3} \lesssim n_i \lesssim 10^{19}$ cm^{-3} and/or of $T \lesssim 300$ K. Outside this range C_{ip} can be roughly approximated by C_0.

(iii) For materials with E_G smaller than Δ_0 plus a few times the thermal energy T, C_{ip} can be well approximated by C_0 in the range of $n_I \gtrsim 10^{17}$ cm^{-3}. In those materials we have $C_{\rm ph} > C_{ip}$.

Though the above conclusion was for p-type materials, it is evident that the same conclusion is drawn also for n-type materials only if we take Δ_0 as zero in (ii) and (iii). It is stressed that the analysis based on the pure collision Auger process leads to erroneous numerical results except for the case (iii) only. Laser diode materials such as GaAs, InP, GaAlAs, and InGaAsP should be analyzed on the basis of the phonon-assisted Auger recombination for nondoped materials or of the impurity- and phonon-assisted Auger recombination for doped materials.

ACKNOWLEDGMENT

The author wishes to express his appreciation to Dr. G. Kano, Dr. I. Teramoto, and Dr. H. Mizuno for their constant encouragement.

APPENDIX A

The reason why the free-particle retarded Green's function can be used to calculate $\Sigma^R_{e\text{-ph}}(l\vec{k},\omega)$ is described here. First of all we calculate $\Sigma^R_{e\text{-ph}}(l\vec{k},\omega)$ up to the first order in the electron-phonon interaction since this is small. Then our discussion should be on the impurity scattering effect on $\Sigma^R_{e\text{-ph}}(l\vec{k},\omega)$. During the phonon emission followed by reabsorption process, an emitted phonon travels over the distance of the order of $c_S\hbar/\omega_{\nu\vec{q}}$, where $2\pi\hbar$ and c_S are the Planck's constant and the sound velocity, respectively. This distance is estimated to be 10^{-8} cm. This is far smaller than the effective radius ($\sim 10^{-6}$ cm) of the impurity potential, out of which an electron is scattered. Therefore, a scattering event by an impurity is far from completion during the one-phonon—emission—reabsorption process.

APPENDIX B

The derivation of the retarded Green's function based on the assumption of the slowly varying impurity potential is discussed. We analyze the retarded Green's function $G^R(l\vec{k},l\vec{k}';\omega)$ in terms of the potential $\Gamma(\vec{r})$ due to all impurities. We have

$$\Gamma(\vec{r}) = \sum_{n=1}^{N_I} U_i(\vec{r}-\vec{R}_n) , \tag{B1}$$

where $U_i(\vec{r}-\vec{R}_n)$ is the potential due to the impurity located at $\vec{R}_n$. Defining the Fourier transform

$$\Gamma(\vec{r}) = \sum_{\vec{q}} \Gamma(\vec{q})\exp(i\vec{q}\cdot\vec{r}) , \tag{B2}$$

we obtain[16]

$$G^R(l\vec{k},l\vec{k}';\omega)=G_0^R(l\vec{k},\omega)[\Delta(\vec{k}-\vec{k}')+\sum_{\vec{q}}\Gamma(\vec{q})G^R(l\vec{q},l\vec{k}';\omega)]\ . \tag{B3}$$

Noting the relation

$$\sum_{\vec{q}}\Gamma(\vec{k}-\vec{q})G^R(l\vec{q},l\vec{k}';\omega)=\sum_{m=0}^{\infty}\frac{1}{m!}\left[i\frac{\partial}{\partial\vec{k}}\cdot\frac{\partial}{\partial\vec{r}}\right]^m\Gamma(\vec{r}=0)G^R(l\vec{k},l\vec{k}';\omega)\ , \tag{B4}$$

the symbolic solution to Eq. (B3) reads

$$G^R(l\vec{k},l\vec{k}';\omega)=\frac{1}{\omega+i\delta-\xi_{l\vec{k}}-\Gamma(i\frac{\partial}{\partial\vec{k}})}\Delta(\vec{k}-\vec{k}')\ , \tag{B5}$$

where $\vec{r}$ in $\Gamma(\vec{r})$ is replaced by the operator $i\partial/\partial\vec{k}$. The equation is rewritten as

$$\begin{aligned}G^R(l\vec{k},l\vec{k}';\omega)&=\frac{1}{V}\int d\vec{r}\frac{1}{\omega+i\delta-\xi_{l\vec{k}}-\Gamma(i\frac{\partial}{\partial\vec{k}})}\exp[i(\vec{k}-\vec{k}')\cdot\vec{r}]\\&=\frac{1}{V}\int d\vec{r}\exp[i(\vec{k}-\vec{k}')\cdot\vec{r}]\frac{1}{\omega+i\delta-\xi_{l\vec{p}}-\Gamma(\vec{r})}1\ ,\end{aligned} \tag{B6}$$

where we define an operator $\vec{p}=\vec{k}+i\partial/\partial\vec{r}$. It is assumed that the potential $\Gamma(\vec{r})$ is effectively a slowly varying function of $\vec{r}$. Then we neglect spatial derivatives of $\Gamma(\vec{r})$ on all orders. We obtain

$$\begin{aligned}G^R(l\vec{k},l\vec{k}';\omega)&=\frac{1}{V}\int d\vec{r}\frac{1}{\omega+i\delta-\xi_{l\vec{k}}-\Gamma(\vec{r})}\exp[i(\vec{k}-\vec{k}')\cdot\vec{r}]\\&=G_0^R(l\vec{k},\omega)\sum_{m=0}^{\infty}[G_0^R(l\vec{k},\omega)]^m\frac{1}{V}\int d\vec{r}[\Gamma(\vec{r})]^m\exp[i(\vec{k}-\vec{k}')\cdot\vec{r}]\\&=G_0^R(l\vec{k},\omega)\sum_{m=0}^{\infty}[G_0^R(l\vec{k},\omega)]^m\sum_{\vec{q}_1,\vec{q}_2,\ldots,\vec{q}_m}\Delta(\vec{Q}_m+\vec{k}-\vec{k}')\prod_{j=1}^{m}\Gamma(\vec{q}_j)\ ,\end{aligned} \tag{B7}$$

where $\vec{Q}_m=\sum_{j=1}^{m}\vec{q}_j$. The last step has been obtained using Eq. (B2) in the integral over $\vec{r}$. An ensemble average, which is taken according to the definition in Eq. (2.9), leads to the Dyson's equation which defines the self-energy. Equation (B7) indicates that we should use only $G_0^R(l\vec{k},\omega)$ as the Green's functions appearing in the diagrams. This is the requirement which results from the assumption of the slowly varying potential. To obtain a more complete Green's function we should replace $G_0^R(l\vec{k},\omega)$ by $G_1^R(l\vec{k},\omega)$. As a result Eq. (2.41) is obtained.

The criterion under which the assumption of the slowly varying potential is justified is found from Eq. (B6) as

$$\frac{\left[\frac{\hbar^2}{2m}\right]^{1/2}\left|\frac{\partial}{\partial\vec{r}}\Gamma(\vec{r})\right|}{|\xi_{l\vec{k}}|^{3/2}}\simeq\frac{\left[\frac{\hbar^2}{2m}\right]^{1/2}\left|\frac{\partial}{\partial\vec{r}}\Gamma(\vec{r})\right|}{\omega^{3/2}}<<1\ , \tag{B8}$$

where spherical energy surface with the effective mass m is assumed for the relevant band. Here only $\xi_{l\vec{k}}$ and ω are measured from the relevant band edge. We see that for low energy the assumption of the slowly varying potential is not justified. Roughly speaking, ω should be larger than the impurity binding energy. In order to effectively have a small value of $|\partial\Gamma(\vec{r})/\partial\vec{r}|$, the potentials due to the nearest-neighbor impurities must overlap each other to an appreciable extent. The condition for this is that the average distance between the nearest-neighbor impurities, which is given[27] by $[3/(2\pi n_i)]^{1/3}$, is smaller than twice the inverse screening length, i.e., $2/\lambda$. This criterion is

$$\frac{1}{2}\left[\frac{3}{2\pi}\right]^{1/3}\frac{n_i^{1/3}}{\lambda}<<1\ . \tag{B9}$$

For degenerate statistics we find $n_i^{1/3}/\lambda\propto n_i^{1/6}$ so that the inequality holds at high doping levels.

APPENDIX C

We calculate $F(\vec{k},0,0)$, which is given from Eq. (3.2) using Eq. (2.63) as

$$F(\vec{k},0,0)=\left[\frac{\epsilon_0}{|Z|e^2\lambda}\right]^2\int_{-\infty}^{\infty}d\omega'\bar{G}^R(\Omega)\mathrm{Re}\bar{G}^R(\Omega)\Theta(\omega')\,, \tag{C1}$$

where an abbreviation $\bar{G}^R(\Omega)=\bar{G}^R(\Omega,\gamma;Z)$ with $\Omega=[\epsilon_0/(|Z|e^2\lambda)](\omega'-\xi_{l\vec{k}})$ is used. Substitution of the expansion

$$\Theta(\omega')=\sum_{n=0}^{\infty}\frac{1}{n!}(\omega'-\xi_{l\vec{k}})^n\frac{\partial_n}{\partial\xi_{l\vec{k}}^n}\Theta(\xi_{l\vec{k}}) \tag{C2}$$

into Eq. (C1) yields

$$F(\vec{k},0,0)=\frac{\epsilon_0}{|Z|e^2\lambda}\sum_{n=0}^{\infty}\frac{1}{n!}\frac{\partial^n}{\partial\xi_{l\vec{k}}^n}\Theta(\xi_{l\vec{k}})\left[\frac{|Z|e^2\lambda}{\epsilon_0}\right]^n\int_{-\infty}^{\infty}d\Omega\,\Omega^n\mathrm{Im}\bar{G}^R(\Omega)\mathrm{Re}\bar{G}^R(\Omega)\,. \tag{C3}$$

Using Eq. (2.64) and the δ function

$$\delta(\xi)=\frac{1}{\pi}\int_{-\infty}^{\infty}d\Omega\cos(\xi\Omega)\,, \tag{C4}$$

the integration over Ω is performed. Defining $g_r(\xi)=\mathrm{Re}g(\xi)$ and $g_i(\xi)=\mathrm{Im}g(\xi)$, the integral in Eq. (C3) becomes

$$-\tfrac{1}{2}\int_0^{\infty}d\xi_1\int_0^{\infty}d\xi_2\exp[\gamma g_r(\xi_1)+\gamma g_r(\xi_2)]$$
$$\times\begin{cases}(-1)^{n-1}\sin[\gamma g_i(\xi_2)-\gamma g_{i(}\xi_1)][\dfrac{\partial^n}{\partial\xi_2^n}\delta(\xi_2-\xi_1)\,, & n\text{ even}\\ (-1)^n\cos[\gamma g_i(\xi_2)-\gamma g_i(\xi_1)]\dfrac{\partial^n}{\partial\xi_2^n}\delta(\xi_2-\xi_1)\,, & n\text{ odd}\,.\end{cases} \tag{C5}$$

This term vanishes when n is even. It is to be noted that from Eq. (C4) we have $(\partial^n/\partial\xi^n)\delta(\xi)|_{\xi=0}=0$ when n is odd. Using this after performing the integration over ξ_2, the term (C5) is found to be $-\pi/4$ if $n=1$ and zero otherwise. Substituting this term into Eq. (C3) we obtain

$$F(\vec{k},0,0)=-\frac{\pi}{4}\frac{\partial}{\partial\xi_{l\vec{k}}}\Theta(\xi_{l\vec{k}})\,. \tag{C6}$$

APPENDIX D

The expression for the dc conductivity is given for a material, which has v equivalent valleys with spherical energy surfaces characterized by the effective mass m. Starting from Kubo's formula,[28] the dc conductivity tensor $\sigma_{\mu\nu}$ is given by

$$\sigma_{\mu\nu}=-\frac{2vi}{\pi V}\frac{e^2\hbar^3}{m^2}\lim_{\omega\to0}\frac{\partial}{\partial\omega}\sum_{\vec{k}_1\vec{k}_2}k_{1\mu}k_{2\nu}\int d\omega'\Theta(\omega')[\,G^A(l\vec{k}_2,l\vec{k}_1;\omega'-\omega)\mathrm{Im}G^R(l\vec{k}_1,l\vec{k}_2;\omega')$$
$$+G^R(l\vec{k}_1,l\vec{k}_2;\omega'+\omega)\mathrm{Im}G^R(l\vec{k}_2,l\vec{k}_1;\omega')]\,. \tag{D1}$$

Here $G^R(lk_1,lk_2;\omega)$ and $G^A(lk_1,lk_2;\omega)$ is the retarded and the advanced Green's function, respectively, which are characterized by Eq. (B3) with $G^A=(G^R)^*$. As shown in I, $G^R(l\vec{k}_1,l\vec{k}_2;\omega)$ can be approximated by the average Green's function defined by Eq. (2.9) assuming that the crystal volume is large enough. Then we obtain

$$\sigma_{\mu\nu}=-\frac{2vi}{\pi V}\frac{e^2\hbar^3}{m^2}\lim_{\omega\to0}\frac{\partial}{\partial\omega}\sum_{\vec{k}}k_\mu k_\nu\int d\omega'\Theta(\omega')[\,G^A(l\vec{k},\omega'-\omega)\mathrm{Im}G^R(l\vec{k},\omega')$$
$$+G^R(l\vec{k},\omega'+\omega)\mathrm{Im}G^R(l\vec{k},\omega')]\,. \tag{D2}$$

The equation is rewritten as

$$\sigma_{\mu\nu}=-\frac{2v}{\pi V}\frac{e^2\hbar^3}{m^2}\sum_{\vec{k}}k_\mu k_\nu\int d\omega\frac{d}{d\omega}\Theta(\omega)[\mathrm{Im}G^R(l\vec{k},\omega)]^2 . \tag{D3}$$

For cubic symmetry we have $\sigma_{\mu\nu}=\Delta(\mu-\nu)\sigma$. After transformation from summation to integration over $\vec{k}$ we obtain

$$\sigma=-\frac{v}{3\pi^3}\frac{e^2\hbar^3}{m^2}\int_0^\infty dk\,k^4\int_{-\infty}^{\infty}d\omega\frac{d}{d\omega}\Theta(\omega)[\mathrm{Im}G^R(l\vec{k},\omega)]^2 . \tag{D4}$$

[1]For review articles see: P. T. Landsberg, Phys. Status Solidi A 41, (1970); A. Haug, in *Festkörperprobleme, Advances in Solid State Physics,* edited by O. Madelung (Pergamon, Braunschweig, 1972), Vol XII, p. 411; R. Conradt, in *Festköreperprobleme, Advances in Solid State Physics,* edited by O. Madelung (Pergamon, Braunschweig, 1972), Vol. XII, p. 449; P. T. Landsberg and M. J. Adams, J. Lumin. 7, 3 (1973).

[2]A. R. Beatie and P. T. Landsberg, Proc. R. Soc. London Ser. A 249, 16 (1959).

[3]M. Takeshima, J. Appl. Phys. 46, 3082 (1975).

[4]L. Huldt, Phys. Status Solidi A 8, 173 (1971).

[5]L. Huldt, Phys. Status Solidi A 24, 221 (1974).

[6]D. Hill and P. T. Landsberg, Proc. R. Soc. London Ser. A 347, 547 (1976).

[7]G. Benz and R. Conradt, Phys. Rev. B 16, 843 (1977).

[8]L. Huldt, Phys. Status Solidi A 33, 607 (1976).

[9]W. Lochmann, Phys. Status Solidi A 40, 285 (1977).

[10]W. Lochmann, Phys. Status Solidi A 42, 181 (1977).

[11]W. Lochmann, Phys. Status Solidi A 45, 423 (1978).

[12]M. Takeshima, Phys. Rev. B 23, 771 (1981).

[13]M. Takeshima, Phys. Rev. B 23, 6625 (1981).

[14]M. Takeshima, J. Appl. Phys. 43, 4114 (1972).

[15]T. Matsubara and Y. Toyozawa, Prog. Theor. Phys. (Kyoto) 26, 739 (1961).

[16]S. Doniach and E. H. Sondheimer, in *Green's Function for Solid State Physicists* (Benjamin, Massachusetts, 1974).

[17]V. L. Bonch-Bruevich, in *Semiconductor and Semimetals,* edited by R. K. Willardson and A. C. Beer (Academic, New York, 1966), Vol. 1, Chap. 4.

[18]A. A. Abrikosov, L. P. Gor'kov, and L. E. Dzyaloshinskii, in *Methods of Quantum Field Theory in Statistical Physics* (Prentice-Hall, Englewood Cliffs, 1965).

[19]V. L. Bonch-Bruevich, Fiz. Tverd. Tela (Leningrad) 4, 2660 (1962) [Sov. Phys.—Solid State 4, 1953 (1963)].

[20]M. J. Katz, Phys. Rev. A 140, 1323 (1965).

[21]V. L. Bonch-Bruevich, in *The Electronic Theory of Heavily Doped Semiconductors* (Academic, New York, 1966).

[22]G. D. Mahan and J. W. Conley, Appl. Phys. Lett. 11, 29 (1967).

[23]A. R. Beatie and G. Smith, Phys. Status Solidi A 19, 577 (1967).

[24]E. O. Kane, in *Semiconductor and Semimetals,* edited by R. K. Willardson and A. C. Beer (Academic, New York, 1966), Vol. 1. Chap. 3.

[25]P. Lawaetz, Phys. Rev. B 4, 3460 (1971).

[26]M. Newberger, in *III-V Semiconducting Compounds* (IFI/Plenum, New York, 1971).

[27]T. Kasuya and S. Koide, J. Phys. Soc. Jpn. 13, 1287 (1958).

[28]R. Kubo, J. Phys. Soc. Jpn. 12, 570 (1957).